Brent's algorithm based new computational approach for accurate determination of single-diode model parameters to simulate solar cells and modules

Fahmi F. Muhammadsharif[1,2,*] Suhairul Hashim[1,3], Shilan S. Hameed[4], S. K. Ghoshal[1], Isam K. Abdullah[5], J. E. Macdonald[6], Mohd Y. Yahya[7]

(1) Department of Physics, Faculty of Science, Universiti Teknologi Malaysia (UTM), 81310 Skudai, Johor, Malaysia
(2) Department of Physics, Faculty of Science and Health, Koya University, 44023 Koya, Kurdistan Region - F.R., Iraq
(3) Centre for Sustainable Nanomaterials (CSNano), Ibnu Sina Institute for Scientific and Industrial Research (ISI-SIR), Universiti Teknologi Malaysia (UTM), 81310 Skudai, Johor, Malaysia
(4) Directorate of Information Technology, Koya University, 44023 Koya, Kurdistan Region -F.R., Iraq
(5) Department of Physics, Salahaddin University, 44001 Erbil, Kurdistan Region-F.R., Iraq
(6) School of Physics and Astronomy, Cardiff University, Cardiff CF24 3AA, UK
(7) Center for Advanced Composite Materials (CACM), Institute for Vehicle Systems & Engineering, Faculty of Mechanical Engineering, Universiti Teknologi Malaysia, 81310 Skudai, Johor, Malaysia

** Corresponding author's email:*
fahmi.fariq@koyauniversity.org
Tel.: +964-7501168841

Abstract

Simulated current-voltage (*I*-*V*) characteristics of photovoltaic (PV) cells and modules are significant for the performance assessment, design and quality control, which are decided by the accurate determination of the intrinsic parameters of the devices. Commonly, a single-diode model is utilized to extract these parameters such as the ideality factor (n), series resistance (R_s), shunt resistance (R_{sh}), saturation current (I_o) and photo-generated current (I_λ). Driven by this idea, a new mathematical manipulation was performed on the single-diode equation that yielded a non-linear formula of R_s. Later, Brent's algorithm was used to precisely estimate R_s at every fine-tuned point of n, thereby all other parameters were determined. The set of parameters that provided the lowest root mean square error (RMSE) between the experimental and simulated *I*-*V* data were chosen to be optimum. The proposed Brent's algorithm (BA) was shown outperform several recently reported computational and

heuristic algorithms that were exploited to mine the single-diode model parameters for solar cells and modules with varied device temperatures and solar irradiation conditions.

Keywords: Solar cells and modules, Parameters extraction, Brent's algorithm, *I-V* simulation, sensitivity analysis.

Abbreviations:

ABC: Artificial Bee Colony

ABSO: Artificial Bee Swarm Optimization

ADA: Adaptive Differential Algorithm

BA: Brent's Algorithm

BMO: Bird Mating Optimizer

CPSO: Chaos Particle Swarm Algorithm

CSO: Cat Swarm Optimization

CWOA: Chaotic Whale Optimization Algorithm

DET: Differential Evolution Technique

EHA-NMS: Eagle-based Hybrid Adaptive Nelder-Mead Simplex Algorithm

ELPSO: Enhanced Leader Particle Swarm Optimization

ER-WCA: Evaporation Rate-based Water Cycle Algorithm

GA: Genetic Algorithm

GGHS: Grouping-based Global Harmony Search

GOTLBO: Generalized Oppositional Teaching Learning Based Optimization

HFAPS: Hybrid Firefly and Pattern Search Algorithm

HS: Harmony Search

IGHS: Innovative Global Harmony Search

ILCOA: Improved Lozi Map based Chaotic Optimization Algorithm

ISCE: Improved Shuffled Complex Evolution

MABC: Modified Artificial Bee Colony

MAE: Mean of Absolute Error

MPCOA: Mutative-scale Parallel Chaos Optimization Algorithm

NM-MPSO: Nelder-Mead and Modified Particle Swarm Optimization

PCE: Population Classification Evolution

PGJAYA: Performance Guided JAYA

PS: pattern search

PSO: particle swarm optimization

R_{cr}-IJADE: Ranking-based Improved Adaptive Differential Evolution

RMSE: Root Mean Squared Error

SA: Simulated Annealing

SAE: Summation of Absolute Error

STLBO: simplified teaching-learning based optimization

Nomenclature:

I_o: saturation current

I_λ: photo-generated current

k_B: Boltzmann's constant (1.381×10^{-23} J/K)

n: ideality factor

q: electron charge (1.602×10^{-19} C)

R_{sh}: shunt resistance

R_s: series resistance

T: temperature in Kelvin

1. Introduction

PV technologies are exploited to convert solar energy into electricity by means of solar cells and modules comprising various architectural designs and active materials (Li et al., 2007; McEvoy et al., 2012; Muhammad and Sulaiman, 2018; Muhammad, Fahmi F et al., 2017; Otte et al., 2006). The easy installation and low maintenance costs of solar energy derived electricity compared to other energy sources make PV technology more convenient and effective. Various factors that affect the performance of PV devices include temperature, solar insolation and aging (Ahmad et al., 2017; Meneses-Rodríguez et al., 2005; Muhammad et al., 2018). Essentially, these factors modify the intrinsic parameters of solar cells and modules, thereby reducing the cell efficiency. Therefore, it is important to model and analyse the current-voltage (*I-V*) characteristics of these devices under diverse operational conditions (Muhammad, Fahmi F. et al., 2017; Xiao et al., 2017).

Over the years, single-diode and double-diode models have been widely studied to mimic the *I-V* characteristics (Humada et al., 2016; Muhammad, Fahmi F. et al., 2017; Villalva, M. G. et al., 2009), wherein the real-world PV behaviour of solar cells and modules have been simulated. The single-diode model has been proven to be accurate approach for the PV devices in terms of simplicity and fast implementation response (Kumar and Kumar, 2017; Orioli and Di Gangi, 2016; Tong and Pora, 2016). This model is represented by an equivalent circuit which is composed of a constant current source connected to an ideal diode in parallel with a shunt resistance driving an external load through a series resistance (Fig. 1(b)).

For the purpose of performance assessment, simulation, design, and quality control, the precise estimation of the solar cells and modules parameters values are significant (Maouhoub, 2018a). Besides, these parameters can be used effectively to predict the energy yield (Müller et al., 2016), to develop algorithm for maximum power point trackers (MPPTs) (Tajuddin et al., 2015; Verma et al., 2016), to develop plug-in hybrid electric vehicles (PHEVs) (Hu et al., 2016), to address the degradation and aging issues in PV devices, (Domanski et al., 2018; Neubauer et al., 2019), and to understand the outdoor operation of PV cells and panels at various environmental conditions (Gaglia et al., 2017). Generally, the manufacturers of PV devices provide a datasheet that includes open circuit voltage (V_{oc}), short circuit current (I_{sc}), maximum rated power (P_m), voltage and current temperature coefficients at standard test condition (STC). However, in the real-world situation the PV devices do not always operate at this standard condition. Often, it is difficult to carry out a steady practical *I-V* measurement over a long-time span and under different outdoor situations. Therefore, it is vital to extract the intrinsic parameters of these devices first before utilizing them in a viable model that is capable of well simulating the *I-V* curve of solar cells and modules at every stage of their utilization and under varied environmental conditions.

Sequentially, various analytical and computational approaches as well as combined strategies were adopted. In the analytical methods, the mathematical equations are manipulated in a way that few characteristic *I-V* points (e.g., V_{oc}, I_{sc}, V_m and I_m) that are provided in the manufacturer's datasheet can be utilized to extract the PV cells and modules parameters (Louzazni and Aroudam, 2015; Park and Choi, 2015; Rasool et al., 2017; Villalva, Marcelo Gradella et al., 2009). Despite a simple implementation, analytical methods neither guarantee the high accuracy nor the realistic estimate of the PV cells and modules parameters (Pindado and Cubas, 2017; Senturk and Eke, 2017; Yadir et al., 2009; Yıldıran and Tacer, 2016). This is because only limited regions of data from the *I-V* curve are considered, resulting in high discrepancies between the simulated and measured *I-V* curve. Alternatively, higher accuracy can be achieved at the expense of increased computational complexity provided the entire *I-V* data is incorporated into the proposed mathematical equations. These derived set of equations are solved by deterministic computational methods including Newton-Raphson, Levenberg–Marquardt, polynomial curve fitting, Lambert-W function and conductivity approach (Chegaar et al., 2001; Chen et al., 2011; Easwarakhanthan et al., 1986; Ma et al., 2014). However, these methods are based on gradient numerical optimization, wherein the proposed equation must be continuous and differentiable over the given interval in order to get the best approximate solution.

Interestingly, stochastic computational optimization based on evolutionary and heuristic algorithms received considerable attention for their capacity of handling nonlinear equations and global search pattern. For instance, differential evolution (DE) technique (Gong and Cai, 2013; Ishaque and Salam, 2011), bird mating optimizer (BMO) (Askarzadeh and dos Santos Coelho, 2015; Askarzadeh and Rezazadeh, 2013b, c), genetic algorithm (GA) (Jervase et al., 2001; Zagrouba et al., 2010), artificial bee colony (ABC) (Oliva et al., 2014) and particle swarm optimization (PSO) (Ye et al., 2009; Yeh, 2009) were successfully utilized to estimate the parameters of PV cells and modules. Basically, these algorithms work on a random selection of the intended parameters simultaneously within a large solution space, ultimately leading to high computational cost and reduced stability. On top, the solution may easily get stuck into the local optimum when the dimension of the objective function is large (Gao et al., 2018). Very recently, researchers have made attempts to better compensate for the limitations of stochastic computational techniques through the establishment of alternative algorithms and internal parametric modifications. Examples of these approaches are PSO with binary constraints (Bana and Saini, 2017), guaranteed convergence PSO (Nunes et al., 2018), improved chaotic whale optimization algorithm (Oliva et al., 2017), improved shuffled complex evolution algorithm (Gao et al., 2018) and hybrid firefly algorithm with pattern search algorithm (HFAPS) (Beigi and Maroosi, 2018). Additionally, with the aim of combining the simplicity of analytical methods and efficiency of computational techniques various hybrid approaches were adopted to estimate the PV cells and modules parameters (Chin et al., 2015; Cubas et al., 2014a; Kumar and Kumar, 2017; Maouhoub, 2018b).

It is known that the performance and accuracy of the techniques used to estimate the single-diode parameters are usually limited by the complexity of their implementation and reproducibility as well as by the methodology of computational approaches that affect the simulated *I-V* curve which deviates from the experimental one. It is because the *I-V* characteristic is highly sensitive to the values of ideality factor and series resistance (Muhammad, Fahmi F. et al., 2017). Thus, special attention must be paid to the initial estimation of the ideality factor and series resistance while implementing the derived equations. To surmount this issue, a new mathematical manipulation is proposed wherein an implicit equation of series resistance (R_s) is initially derived. Later, Brent's Algorithm (BA) (Brent, 2013) is used to determine the roots of the non-linear equations with assured convergence. This could accurately estimate R_s at every fine-tuned point of n. Finally, complete set of values of R_s and n were considered to extract the rest of the parameters. The set of parameters which provided the lowest root mean square error (RMSE) between the experimental and simulated *I-V* data were selected as the optimum solution. The proposed BA was deployed via MATLAB programming code to build a user-friendly software application which could automatically perform the process of parameters extraction.

Simple implementation of this technique via the utilization of few viable equations and high accuracy of the simulated *I-V* compared to that of the experimental ones at various environmental conditions can be featured as two main contributions of the current work. The proposed method required a set of *I-V* data without the need of providing PV parameters manually. The method itself used the extrapolation fitting to estimate the PV parameters prior to the initialization. The rest of the paper describes the methodology of the mathematical manipulations and the implementation of BA used to extract accurately the parameters and *I-V* curve. Subsequently, the method was validated on both of solar cells and modules operated under different device temperatures and solar irradiations. Finally, the main conclusions of the research were drawn.

2. Methodology

2.1. Mathematical Formalism

Figs. 1(a-c) show the structure of a typical photovoltaic device, its equivalent circuit and standard *I-V* characteristics under dark and illumination, respectively. The light activated current source (I_λ) defines the amount of current generated in the cell when exposed to sunlight energy. The net current in the connected load determines the final characteristic current of the device, which is represented by.

$$I = I_\lambda - I_o \left[\exp\left(\frac{V + IR_s}{nV_t}\right) - 1\right] - \frac{(V + IR_s)}{R_{sh}} \qquad (1)$$

where n is the ideality factor of the solar cell signifying the charge transport efficiency of the device, I_o is the saturation (generation) current of the diode under dark conditions, V_t is the thermal voltage represented by $k_B T/q$, k_B is the Boltzmann's constant, T is the temperature in Kelvin, q is the elementary charge and R_s and R_{sh} are the respective series and shunt resistance. For a PV module, $(V + IR_s) = (V/N_s + IR_s)$ since PV module is composed of N_s series connected cells. Consequently, the denominator of the exponent part in the equation is involved with N_s. Thus, during the numerical iterations, ($N_s \times n$) should be considered instead of n. The validity of single-diode model is dependent on the applicability of the principle of superposition, whereby the effect of illumination is simply to displace the current by an amount equal to I_λ everywhere along the *I-V* curve and whereby all other terms in Eq. (1) retain their unilluminated and/or unbiased values (Del Cueto and Rummel, 2005).

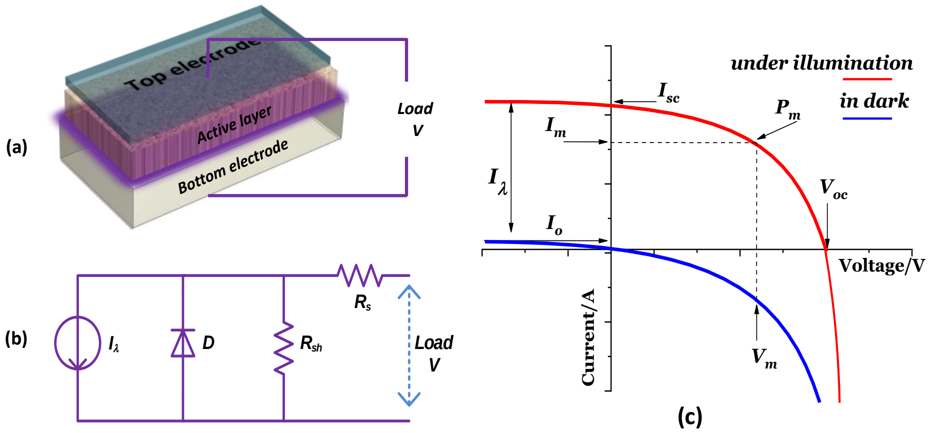

Fig. 1. A prototype structure of PV cells (a), the equivalent circuit used to simulate *I*-*V* curve of PV cells based on single-diode model (b) and their standard *I*-*V* characteristics (c).

Based on the *I*-*V* characteristic curves shown in Fig. 1(c), three boundary conditions can be considered at the points of open circuit voltage (V_{oc}), short circuit current (I_{sc}) and maximum power (P_m) such that Eq. (1) takes the form (Chaibi et al., 2018):

$$0 = I_\lambda + I_o - I_o \exp\left(\frac{V_{oc}}{nV_t}\right) - \frac{V_{oc}}{R_{sh}} \qquad (2)$$

$$I_{sc} = I_\lambda + I_o - I_o \exp\left(\frac{R_s I_{sc}}{nV_t}\right) - \frac{R_s I_{sc}}{R_{sh}} \qquad (3)$$

$$I_m = I_\lambda + I_o - I_o \exp\left(\frac{R_s I_m + V_m}{nV_t}\right) - \frac{R_s I_m}{R_{sh}} - \frac{V_m}{R_{sh}} \qquad (4)$$

Subtracting Eq. (2) from Eq. (3), the saturation current (I_o) was obtained:

$$I_o = \frac{I_{sc} - \frac{V_{oc}}{R_{sh}} + \frac{R_s}{R_{sh}} I_{sc}}{\exp\left(\frac{V_{oc}}{nV_t}\right) - \exp\left(\frac{R_s I_{sc}}{nV_t}\right)} \qquad (5)$$

By neglecting $\exp\left(\frac{R_s I_{sc}}{nV_t}\right)$ one can simplify the calculations wherein corresponding Eq. (3) and Eq. (5) reduced to:

$$I_{sc} = I_\lambda + I_o - \frac{R_s I_{sc}}{R_{sh}} \qquad (6)$$

$$I_o = \frac{I_{sc} - \frac{V_{oc}}{R_{sh}} + \frac{R_s}{R_{sh}} I_{sc}}{\exp\left(\frac{V_{oc}}{nV_t}\right)} \qquad (7)$$

Using Eq. (6) and Eq. (4) one achieves:

$$I_\lambda + I_o = I_{sc} + \frac{R_s I_{sc}}{R_{sh}} = I_m + I_o \exp\left(\frac{R_s I_m + V_m}{nV_t}\right) + \frac{R_s I_m}{R_{sh}} + \frac{V_m}{R_{sh}} \qquad (8)$$

By substituting Eq. (7) into Eq. (8) and solving for R_{sh} one gets:

$$R_{sh} = \frac{R_s I_{sc} A - V_{oc} A - R_s I_{sc} + R_s I_m + V_m}{I_{sc} - I_m - I_{sc} A} \qquad (9)$$

where $A = \exp\left(\frac{R_s I_m + V_m}{nV_t}\right)$. Another explicit relation can also be derived for R_{sh} by applying a boundary condition at the maximum power point (P_m) on the power-voltage (P-V) curve as depicted in Fig. 2. When a solar cell operates at P_m, maximum power is delivered to the external load. In this situation, the total internal resistance (R_T) of the solar cell (equivalent circuit) corresponds to the resistance of the external load (R_L):

$$R_T = R_L = \frac{V_m}{I_m} \qquad (10)$$

Based on the equivalent circuit, Eq. (10) can be applicable at the point of P_m ($I_m \times V_m$) regardless of the temperature and irradiation conditions as long as the load resistance is exactly matched to the total internal resistance:

$$\frac{R_{sh} \acute{R_d}}{R_{sh} + \acute{R_d}} + R_s = \frac{V_m}{I_m} \qquad (11)$$

where $\acute{R_d}$ is the dynamic resistance of the diode at P_m and it is determined from the first derivative of the diode voltage with respect to its current. A non-linear load line is noticeable in Fig. 2, which arises due to the nonlinear increase in the potential difference on R_L with the increase of R_L value across the PV devices.

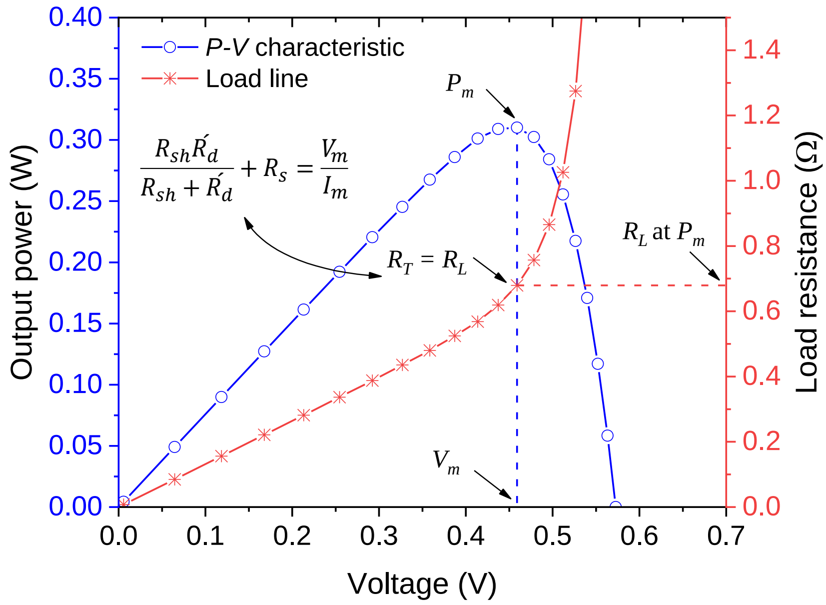

Fig. 2. *P-V* curve and load line for a typical solar cell, revealing maximum power delivery to the load at V_m.

$$\acute{R}_d = \left.\frac{dV_D}{dI_D}\right|_{P_m} = \frac{nV_t}{I_o exp(\frac{R_sI_m + V_m}{nV_t})} \qquad (12)$$

Substituting Eq. (12) into Eq. (11) and performing few mathematical manipulations one obtains:

$$I_o \exp\left(\frac{R_sI_m + V_m}{nV_t}\right) = \frac{nV_t(I_m - \frac{V_m}{R_{sh}} + \frac{R_sI_m}{R_{sh}})}{V_m - R_sI_m} \qquad (13)$$

Similarly, by subtracting Eq. (2) from Eq. (4) and combining Eq. (7) one gets:

$$I_o \exp\left(\frac{R_sI_m + V_m}{nV_t}\right) = I_{sc} - I_m + \frac{R_s}{R_{sh}}(I_{sc} - I_m) - \frac{V_m}{R_{sh}} \qquad (14)$$

From Eq. (13) and Eq. (14) one achieves the second explicit form of R_{sh} given by:

$$R_{sh} = \frac{V_m^2 + R_s^2(I_{sc}I_m - I_m^2) + R_s(nV_tI_m - I_{sc}V_m) - nV_tV_m}{R_s(I_m^2 - I_{sc}I_m) + V_m(I_{sc} - I_m) - nV_tI_m} \qquad (15)$$

By combining Eq. (9) and Eq. (15) it is possible to derive a stand-alone implicit relation for R_s represented by:

$$R_s = \frac{V_{oc}V_m(I_{sc} - I_m) + nV_t(I_{sc}V_m - I_mV_{oc}) - V_m^2 I_{sc} + \frac{nV_tV_m(2I_m - I_{sc})}{A}}{I_{sc}I_m(V_{oc} - V_m) - I_m^2 V_{oc}} \qquad (16)$$

To predict the accuracy of the proposed method and to derive the cost function, summation of absolute error (SAE), mean of absolute error (MAE) and root mean squared error (RMSE) were calculated via the respective relations:

$$SAE = \sum_{i=1}^{k} \left| I_i^{meas} - I_i^{sim} \right| \qquad (17)$$

$$MAE = \frac{1}{k}\sum_{i=1}^{k} |(I_i^{meas} - I_i^{sim})| \qquad (18)$$

$$RMSE = \sqrt{\frac{1}{k}\sum_{i=1}^{k} (I_i^{meas} - I_i^{sim})^2} \qquad (19)$$

where k is the number of elements in the measured *I-V* set, I_i^{meas} and I_i^{sim} are the *i*th measured and simulated current, respectively.

2.2. Brent's Algorithm

Brent's algorithm (BA) is a root-finding algorithm combining the inverse quadratic interpolation and methods of bisection as well as secant. It often uses the potentially fast-converging secant method or inverse quadratic interpolation, sometimes relies on the more robust bisection method if necessary. Therefore, BA has been purposely built to get benefit from the efficiency of the bisection method and low computational cost of the secant or inverse quadratic interpolation techniques. Fig. 3 illustrates a flowchart of BA used to find the zero of a function through sign changes in a given interval. In the present work, BA was successfully utilized to solve Eq. (16) for extracting the PV parameters and performing *I-V* simulation. BA is guaranteed to converge for any function in a reasonable number of steps (Brent, 1971). BA can be used by means of *fzero* command in MATLAB, which is dedicated to find the zero of a function of single variable denoted by x based on a user-supplied initial guessed value x_0 (Magrab et al., 2007).

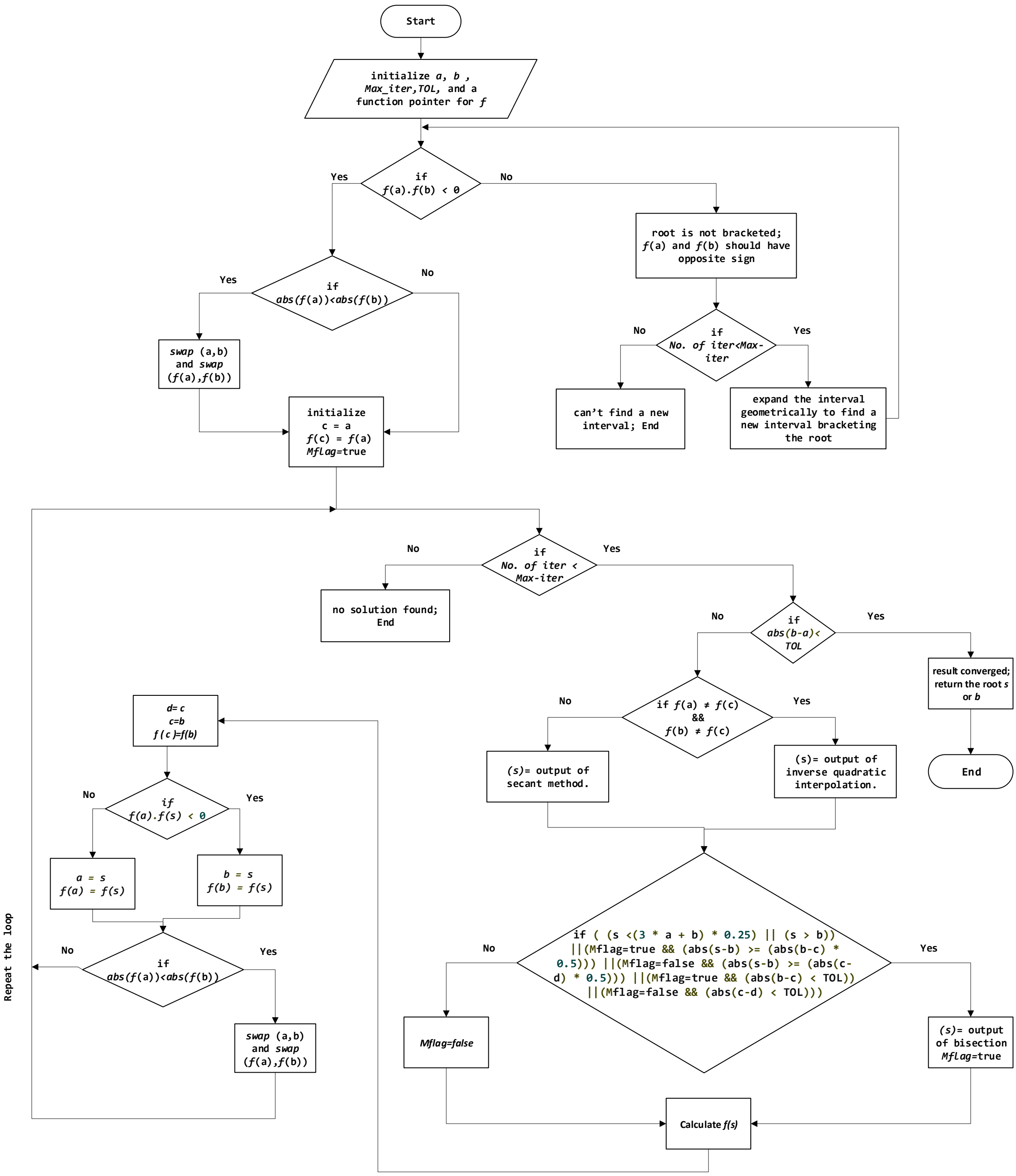

Fig. 3. Flowchart of Brent's algorithm used for efficient extraction of solar cells and modules parameters.

2.3. Implementation Procedure

The implementation steps for solar cells and modules parameters extraction using the proposed BA is presented in Fig. 4. First, the PV parameters (V_m, I_m, V_{oc} and I_{sc}) were computed from the given *I-V* data using polynomial, exponential and polynomial curve fittings around the points where P_m, I_{sc} and V_{oc} are located, respectively. Then, a set of n was generated in the selected range of 0.5 to 7. Such choice guaranteed an accurate extraction of n for almost every kind of solar cells and modules because some devices display relatively high n. In each iteration, one value of n was chosen and Eq. (16) was solved to determine the most accurate value of R_s using BA (see Fig. 3). Meanwhile, Eq. (15), Eq. (5) and Eq. (2) were respectively used to estimate the value of R_{sh}, I_o and I_λ. Next, the extracted parameters from every iteration were used to produce a bunch of simulated *I-V* curve. Finally, the set of parameters which belonged to the simulated *I-V* curve presented the minimum cost function, implying lowest RMSE between the measured and simulated *I-V* data, was chosen as the best solution.

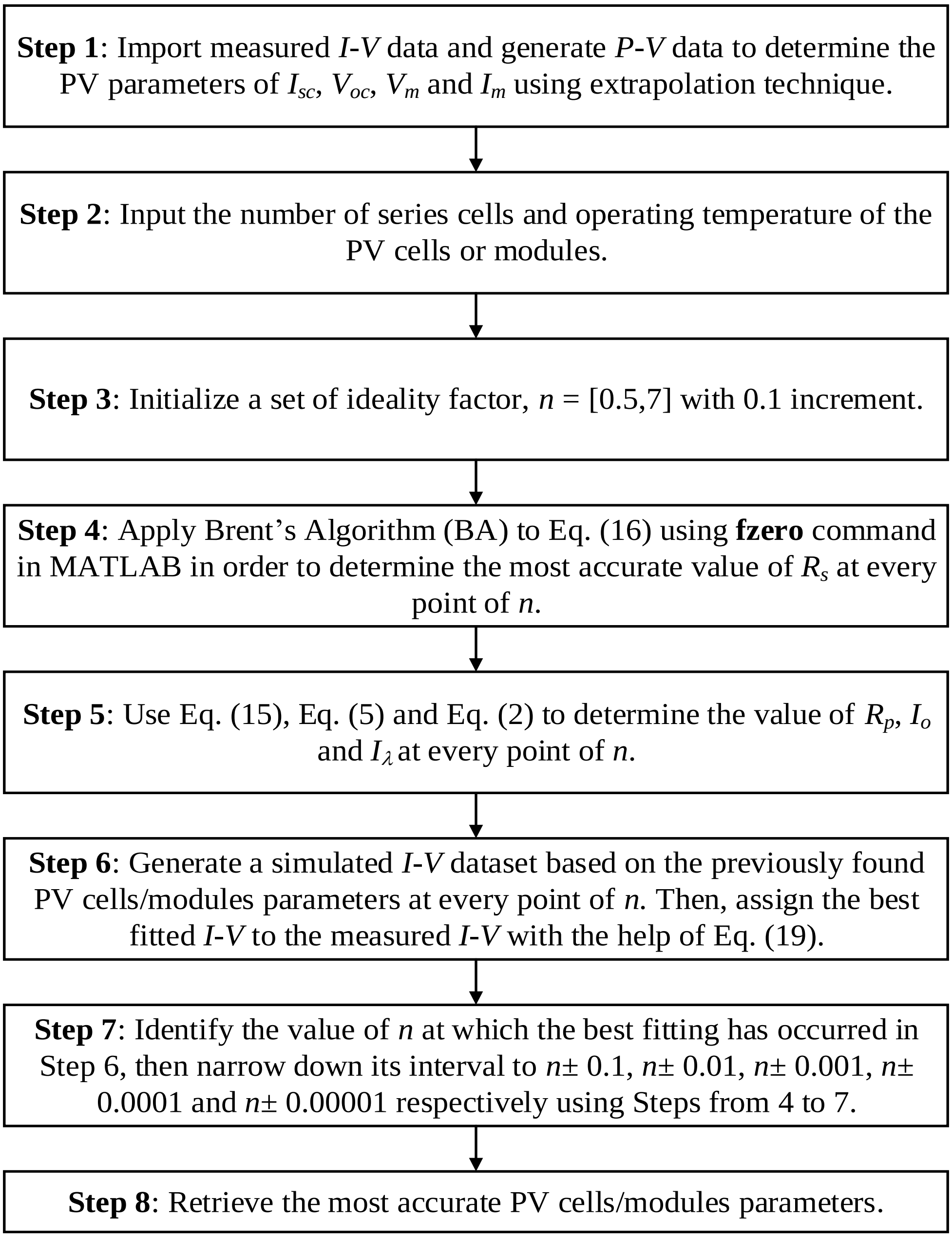

Fig. 4. Implementation steps for determining accurately the values of PV cells and modules parameters using BA to estimate the R_s.

3. Results and Discussion

Validation and assessment of the proposed BA was performed on eight different PV devices (four PV cells and six PV modules) at different device temperatures and solar irradiations. Consequently, the extracted PV cells and modules parameters were recorded and utilized to generate simulated *I-V* data for each type of the device. The correctness and robustness of the proposed method was tested by comparing with the existing art of the techniques reported in the literature.

3.1 Validation on PV Cells

The validation and accuracy of the proposed BA was performed on two different solar cells such as R.T.C. France silicon and PVM 752 GaAs. The measured *I-V* data for R.T.C. France solar cell with a 57 mm-diameter operating at cell temperature (T) of 33 °C and irradiation of 1000 W/m^2 was selected (Easwarakhanthan et al., 1986). Meanwhile, the PVM 752 GaAs thin film solar cell was operated at 25 °C and irradiation of 1000 W/m^2, wherein the measured *I-V* data was obtained (Jordehi, 2018). The BA based results for R.T.C. France single-crystalline solar cell are shown in Fig. 5, while the measured and calculated *I-V* dataset is provided as Appendix A. Clearly, the simulated currents agreed very good well with the experimental ones. Fig. 5(a) showed that the proposed method is more sensitive to the PV parameters of V_m and I_m, where the simulated currents were more deviated from that of the measured currents around P_m. This can be ascribed to the effect of polynomial fitting which was used to extract the value of V_m and I_m from the experimental *I-V* data. Besides, Fig. 5(b) further revealed the closeness between the simulation and experimental results of the *I-V* data.

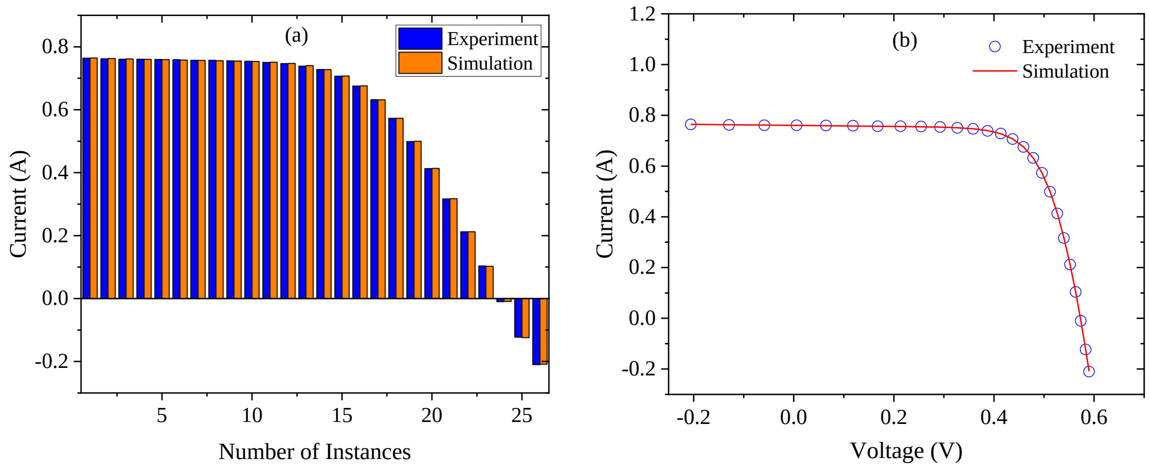

Fig. 5. Simulation (calculated) and experimental (measured) currents for single-diode model of R.T.C. France solar cell (a) and their *I-V* curves (b).

The accuracy of simulated *I-V* data were compared to those reported in the literature. It was found that BA outperformed several recently reported methods as depicted in Table 1, wherein the uncertainty percentage in the extracted parameters is also given. Additionally, the extracted parameters of R.T.C. France solar cell using the proposed technique were compared to those determined by some of other reported methods. The error between simulation and experimental *I-V* data in terms of SAE, MAE and RMSE indicated an excellent accuracy for the proposed BA which was attributed to the strong reliance of accurate determination of the PV cells and modules parameters. In short, the proposed approach achieved lowest RMSE value of (7.7896±0.005%) $\times 10^{-4}$ for the R.T.C. France solar cell, which was lower than those obtained by the existing state of the art techniques such as PGJAYA, ILCOA, HFAPS and ER-WCA.

Table 1. Comparison of different parameter extraction methods for single-diode model of R.T.C. France solar cell worked at 33 °C and 1000 W/m².

Method	n	R_s (Ω)	R_{sh} (Ω)	I_λ (A)	I_o (μA)	SAE	MAE	RMSE
BA (proposed)	1.4732	0.0367±0.002%	52.4722	0.7608±0.004%	0.2983±0.006%	(1.7789±0.002%) $\times 10^{-2}$	6.8420×10^{-4}	**(7.7896±0.005%) $\times 10^{-4}$**
PGJAYA (Yu et al., 2019)	1.4812	0.0364	53.7185	0.7608	0.3230	NA	NA	9.8602×10^{-4}
ILCOA (Pourmousa et al., 2019)	1.4811	0.0364	53.7187	0.7608	0.3230	NA	NA	9.8602×10^{-4}
HFAPS (Beigi and Maroosi, 2018)	1.4811	0.0364	53.6784	0.7608	0.3226	NA	NA	9.8602×10^{-4}
ER-WCA (Kler et al., 2017)	1.4811	0.0364	53.6910	0.7608	0.3227	NA	6.7985×10^{-4}	9.8602×10^{-4}
DET (Chellaswamy and Ramesh, 2016)	1.4870	0.0360	54.5320	0.7510	0.3150	NA	NA	9.3000×10^{-4}
IJAYA (Yu et al., 2017)	1.4811	0.0364	53.7595	0.7608	0.3228	NA	NA	9.8603×10^{-4}
ISCE (Gao et al., 2018)	1.4812	0.0364	53.7185	0.7608	0.3230	1.7704×10^{-2}	NA	9.8602×10^{-4}
EHA-NMS (Chen, Z. et al., 2016)	1.4812	0.0364	53.7185	0.7608	0.3230	1.7704×10^{-2}	NA	9.8602×10^{-4}
R_{cr}-IJADE (Gong and Cai, 2013)	1.4812	0.0364	53.7185	0.7608	0.3230	1.7704×10^{-2}	NA	9.8602×10^{-4}
PCE (Zhang et al., 2016)	1.4811	0.0364	53.7185	0.7608	0.3230	NA	NA	9.8602×10^{-4}
ABC (Oliva et al., 2014)	1.4817	0.0364	53.6433	0.7608	0.3251	NA	8.3034×10^{-4}	9.8620×10^{-4}
GOTLBO (Chen, X. et al., 2016)	1.4838	0.0363	54.1154	0.7608	0.3316	NA	NA	9.8744×10^{-4}
CSO (Guo et al.,	1.4812	0.0364	53.7185	0.7608	0.3230	NA	6.7968×10^{-4}	9.8602×10^{-4}

2016)								
STLBO (Niu et al., 2014)	1.4811	0.0364	53.7187	0.7608	0.3230	NA	8.2900×10^{-4}	9.8602×10^{-4}
ABC-DE (Hachana et al., 2013)	1.4799	0.0364	53.7185	0.7608	0.3230	NA	NA	9.8602×10^{-4}
BMO (Askarzadeh and Rezazadeh, 2013b)	1.4817	0.0364	53.8716	0.7608	0.3248	NA	4.6210×10^{-3}	9.8608×10^{-4}
NM-MPSO (Hamid et al., 2016)	1.4812	0.0364	53.7222	0.7608	0.3230	NA	4.5980×10^{-3}	9.8602×10^{-4}
MABC (Jamadi et al., 2016)	1.4814	0.0364	53.4000	0.7608	0.3213	NA	8.3118×10^{-4}	9.8610×10^{-4}
GGHS (Askarzadeh and Rezazadeh, 2012)	1.4822	0.0363	53.0647	0.7609	0.3262	NA	4.6000×10^{-3}	9.9097×10^{-4}
ABSO (Askarzadeh and Rezazadeh, 2013a)	1.4758	0.0366	52.2903	0.7608	0.3062	NA	NA	9.9124×10^{-4}
IGHS (Askarzadeh and Rezazadeh, 2012)	1.4874	0.0361	53.2845	0.7608	0.3435	NA	NA	9.9306×10^{-4}
CPSO (Wei et al., 2011)	1.5033	0.0354	59.0120	0.7607	0.4000	NA	1.6800×10^{-1}	1.3900×10^{-4}
CWOA (Oliva et al., 2017)	1.4812	0.0364	53.7987	0.7608	0.3239	NA	8.2800×10^{-4}	9.8604×10^{-4}
GA (Jervase et al., 2001)	1.5750	0.0290	42.3730	0.7620	0.8090	NA	NA	1.9100×10^{-2}

NA: not available in the literature

Following the earlier procedures, the solar cell parameters of the second PV cell was determined and BA model was validated on PVM 752 GaAs thin film solar cell (Jordehi, 2018). After determining the cell parameters, the simulated currents were compared with the experimental ones (Appendix B). Fig. 6(a) and Fig. 6(b) displays the excellent fit of the simulated data with the measured one, where a trivial deviation around the maximum power point was observed with naked eyes. This might be referred to the effect of the extrapolated method that was applied to identify the values of V_m and I_m. The calculated/simulated *I-V* data were compared with those reported in the literature. It was concluded that BA performed excellently to determine the PV parameters of the PVM 752 GaAs with lowest RMSE of (2.1049±0.007%) $\times10^{-4}$ (see Table 2), wherein the uncertainty percentage in the extracted parameters is also given. The tiny values of SAE, MAE and RMSE clearly signified excellent competitive accuracy for the proposed method that strongly relied on the accurate determination of PV cells parameters.

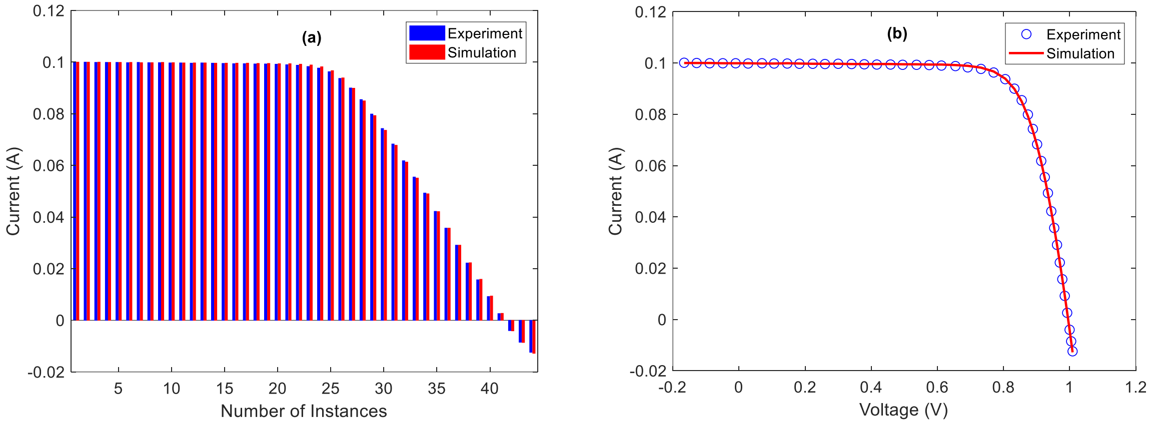

Fig. 6. Simulated and experimental currents for single-diode model of PVM 752 GaAs solar cell (a) and their *I-V* curves (b).

Table 2. Comparison of different parameter extraction methods for single-diode model of PVM 752 GaAs thin film cell operated at 25 °C and 1000 W/m^2.

Method	*n*	R_s (Ω)	R_{sh} (Ω)	I_λ (A)	I_o (pA)	SAE	MAE	RMSE
BA (proposed)	1.7341±0.001%	0.6165±0.007%	684.5160	0.0999±0.007%	19.4226	(7.4258±0.008%) ×10^{-3}	1.6877×10^{-4}	**(2.1049±0.007%) ×10^{-4}**
ABC (Jordehi, 2018)	1.7742	0.5000	100.0000	0.1033	32.000	NA	NA	2.0412×10^{-3}
BSA (Jordehi, 2018)	1.8586	0.5000	100.0000	0.1039	84.900	NA	NA	2.1469×10^{-3}
CPSO (Wei et al., 2011)	1.6171	0.3466	14.2400	0.1165	0.000	NA	NA	2.5400×10^{-2}
ELPSO (Jordehi, 2018)	1.7686	0.1591	14.4300	0.1150	0.000	NA	NA	2.5400×10^{-2}

3.2 Validation on PV Modules

In addition to PV cells, six different solar modules were also tested under various environmental conditions to extract the parameters and further validation of the proposed BA technique. The first module was Photowatt-PWP201 comprising of 36 polycrystalline silicon cells in series that operated at 45 °C and 1000 W/m^2. The experimental *I-V* data of this module was obtained following the earlier work (Easwarakhanthan et al., 1986). The simulated *I-V* results are depicted in Appendix C, while the extracted parameters along with methods accuracy are summarized in Table 3, wherein the uncertainty percentage in the extracted parameters is also given.

Fig. 7 shows the curve fitting results for Photowatt-PWP201 solar module obtained by the proposed method. The calculated currents are shown to tally very well with the measured ones in both high and low voltage regions. With this method of simulation and parameters extraction, a lowest RMSE of (2.1256±0.002%) $\times 10^{-3}$ was achieved for Photowatt-PWP201 solar module, implying higher accuracy of BA compared to that of several reported methods (Table 3). Moreover, the proposed technique does not require any manual initialization of parameters. Conversely, some optimization problems need to be continuously perturbed through parameters variation, thereby increasing the computational cost and leading to an entrapment in the local optimum.

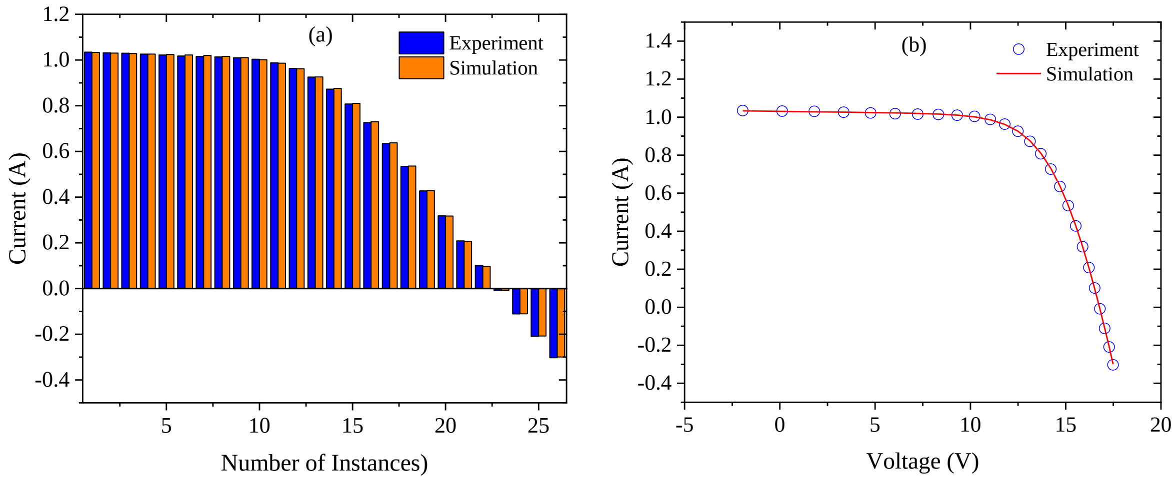

Fig. 7. Simulated and experimental currents for single-diode model of Photowatt-PWP201 solar module (a) and their *I-V* curves (b).

Table 3. Comparison of various parameter extraction methods for single-diode model of Photowatt-PWP201 solar module comprising 36 polycrystalline silicon cells in series worked at 45 °C and 1000 W/m^2.

Method	n	R_s (Ω)	R_{sh} (Ω)	I_λ (A)	I_o (μA)	SAE	MAE	RMSE
BA (proposed)	1.3356±0.006%	1.2184±0.003%	761.4900	1.0323±0.003%	2.9983±0.007%	43.0390$\times 10^{-3}$	(1.6553±0.004%) $\times 10^{-3}$	**(2.1256±0.002%) $\times 10^{-3}$**
PGJAYA (Yu et al., 2019)	1.3512	1.2013	981.8545	1.0305	3.4818	NA	NA	2.4250$\times 10^{-3}$
HFAPS (Beigi and Maroosi, 2018)	1.3512	1.2013	984.2813	1.0305	3.4842	NA	NA	2.4251$\times 10^{-3}$
ER-WCA (Kler et al., 2017)	1.3553	1.1963	961.0530	1.0306	3.6146	NA	1.5829$\times 10^{-3}$	2.3558$\times 10^{-3}$
IJAYA (Yu et al., 2017)	1.3508	1.2016	977.3752	1.0305	3.4703	NA	NA	2.4251$\times 10^{-3}$

ISCE (Gao et al., 2018)	1.3512	1.2013	981.9823	1.0305	3.4823	41.7879×10^{-3}	NA	2.4251×10^{-3}
EHA-NMS (Chen, Z. et al., 2016)	1.3512	1.2013	981.9823	1.0305	3.4823	41.7879k×10^{-3}	NA	2.4250×10^{-3}
MPCOA (Yuan et al., 2014)	1.3474	1.2030	849.6927	1.0319	3.3737	21.5100×10^{-3}	2.6100×10^{-3}	2.4250×10^{-3}
Newton (Easwarakhanthan et al., 1986)	1.3458	1.2057	555.5556	1.0318	3.2875	NA	8.3200×10^{-3}	7.8050×10^{-1}
PS (AlRashidi et al., 2011)	1.3414	1.2053	714.2857	1.0313	3.1756	NA	5.3000×10^{-3}	1.1800×10^{-1}
IP (Tong and Pora, 2016)	1.3106	1.2744	715.8240	1.0333	2.3326	NA	1.7600×10^{-3}	NA
GA (AlRashidi et al., 2011)	1.3496	1.1968	555.5560	1.0441	3.4360	15.3479×10^{-2}	8.8800×10^{-3}	NA

The performance of the proposed algorithm assessed by extracting the parameters of a mono-crystalline solar module (LEYBOLD 664 431) and simulating its *I-V* characteristics. This solar module was obtained from Leybold GmbH., which comprised of 20 series cells and operated at module temperature of 24 ^{o}C under outdoor sunlight intensity of 360 W/m^2. The experimental *I-V* data was recorded manually via digital multimeters of type VC-920/Voltcraft with error ±0.08% and 1% for the DC voltage and current, respectively, while a potentiometer was utilized as a variable load across the module terminals. As this solar module was tested under outdoor condition, there has been some variations/noises in the practically measured *I-V* data. The simulated results obtained using BA are summarized in Table 4. The extracted parameters were n = 1.2688±0.001%, R_s = 6.3944±0.005% Ω, R_{sh} = 1973.35 Ω, I_λ = 0.1544±0.008% A and I_o = 2.5087±0.008% nA. The BA revealed outstanding performance with a lowest RMSE value of (8.3838±0.007%) ×10^{-4}.

Table 4. Calculated/simulated results of BA for single-diode model of Leybold Solar Module (LEYBOLD 664 431) comprising of 20 series cells worked at 24 ^{o}C and outdoor sunlight intensity of 360 W/m^2.

Instance	Voltage (V)	Experimental Current (A)	Simulated Current (A)	Absolute Error
1	0.000	0.1540	0.1540	0.0000
2	0.370	0.1540	0.1538	0.0002
3	0.670	0.1540	0.1537	0.0003
4	0.990	0.1540	0.1535	0.0005
5	1.310	0.1530	0.1533	0.0003
6	1.670	0.1530	0.1531	0.0001
7	3.100	0.1520	0.1524	0.0004
8	4.600	0.1520	0.1517	0.0003
9	6.000	0.1510	0.1508	0.0002

10	7.450	0.1500	0.1492	0.0008
11	8.550	0.1440	0.1443	0.0003
12	9.300	0.1340	0.1339	0.0001
13	9.750	0.1230	0.1218	0.0012
14	10.040	0.1120	0.1108	0.0012
15	10.260	0.1020	0.1004	0.0016
16	10.990	0.0550	0.0541	0.0009
17	11.200	0.0370	0.0376	0.0006
18	11.310	0.0281	0.0284	0.0003
19	11.370	0.0227	0.0233	0.0006
20	11.410	0.0190	0.0198	0.0008
21	11.440	0.0160	0.0172	0.0012
22	11.460	0.0142	0.0154	0.0012
23	11.480	0.0127	0.0136	0.0009
24	11.500	0.0120	0.0118	0.0002
25	11.550	0.0060	0.0073	0.0013
26	11.580	0.0030	0.0046	0.0016
27	11.600	0.0020	0.0027	0.0007
28	11.610	0.0010	0.0018	0.0008
29	11.620	0.0010	0.0009	0.0001
30	11.630	0.0006	0.0000	0.0006
31	11.632	0.0003	0.0004	0.0001
32	11.633	0.0002	-0.0003	0.0005
33	11.636	0.0001	-0.0002	0.0003
34	11.640	0.0001	-0.0001	0.0002
35	11.650	0.0000	-0.0020	0.0020
	SAE	$(2.4249\pm0.001\%)\times10^{-2}$		
	MAE	$(6.9283\pm0.001\%)\times10^{-4}$		
	RMSE	$(8.3838\pm0.007\%)\times10^{-4}$		

Fig. 8 shows that the sensitivity of the proposed approach to the maximum power point (MPP) on the *I-V* curve is more pronounced in solar modules compared to that of the solar cells (Figs. 5 and 6). Noteworthy, a superior extraction of single-diode parameters can be achieved by the proposed BA method compared to the other computational and heuristic algorithms.

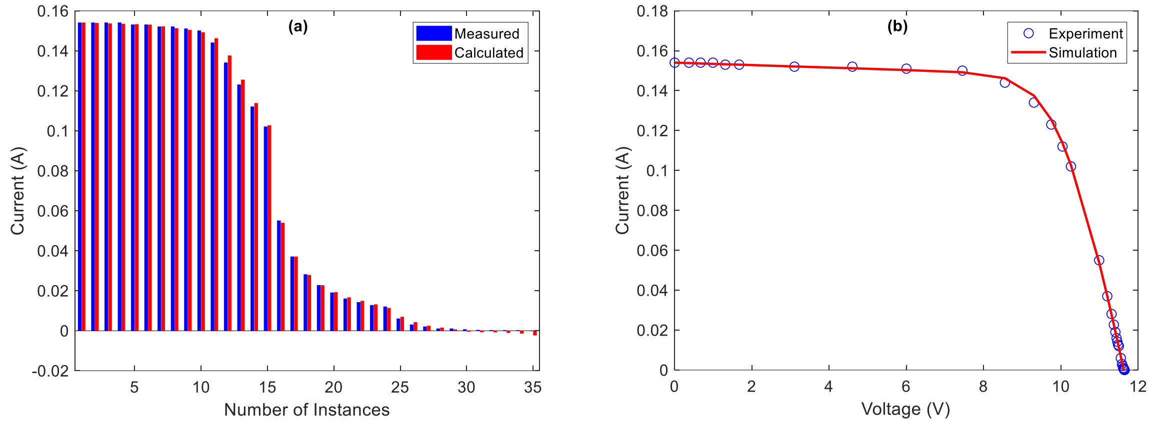

Fig. 8. Simulated and experimental currents for single-diode model of Leibold Solar Module (LEYBOLD 664 431) (a) and their *I-V* curves (b).

The third investigated module was a four series cells-based polycrystalline PV module (STE 4/100) purchased from Leybold GmbH. Experimental *I-V* data of this cell was measured at module temperature of 22 ^{o}C under indoor light intensity of 900 W/m^2. The measured *I-V* and simulated *I-V* dataset obtained by the proposed BA along with the possible errors are enlisted in Table 5. Interestingly, the proposed method could effectively model the *I-V* behaviour of the module with a RMSE of (3.3392±0.004%) ×10^{-4}. Consequently, the extracted parameters of this solar module were discerned to be n = 1.0304, R_s = 2.5567±0.008% Ω, R_{sh} = 2184.82 Ω, I_λ = 0.0264±0.005% A and I_o = 0.1298±0.001% nA. For commercial solar modules the estimated R_s presents lumped series resistance which is the total resistance of electrodes, Ohmic contact resistance and bulk resistance of the module active layer.

Table 5. Results of BA for single-diode model of Leybold Solar Module (STE 4/100) comprised of 4 series cells operated at 22 ^{o}C under light intensity 900 W/m^2.

Instance	Voltage (V)	Experimental Current (A)	Simulated Current (A)	Absolute Error
1	0.00	0.0264	0.0264	0.0000
2	0.10	0.0264	0.0264	0.0000

3	0.30	0.0263	0.0263	0.0000
4	0.50	0.0262	0.0262	0.0000
5	0.70	0.0261	0.0261	0.0000
6	0.90	0.0260	0.026	0.0000
7	1.00	0.0259	0.026	0.0001
8	1.10	0.0258	0.0259	0.0001
9	1.20	0.0257	0.0259	0.0002
10	1.30	0.0256	0.0258	0.0002
11	1.40	0.0253	0.0256	0.0003
12	1.50	0.0252	0.0253	0.0001
13	1.60	0.0247	0.0247	0.0000
14	1.70	0.0232	0.0231	0.0001
15	1.80	0.0189	0.0196	0.0007
16	1.90	0.0121	0.0125	0.0004
17	1.95	0.0081	0.0071	0.0010
18	2.00	0.0000	0.0003	0.0003
	SAE	$(3.5644\pm0.008\%)\times10^{-3}$		
	MAE	$(1.9802\pm0.007\%)\times10^{-4}$		
	RMSE	$(3.3392\pm0.004\%)\times10^{-4}$		

3.3 Modelling using BA under Different Environmental Conditions

The performance assessment and validation of the proposed BA at different device temperatures and various solar irradiations were conducted on three commercial solar modules including KC200GT (multi-crystalline), SX3200N (multi-crystalline) and 1STH-235WH (mono-crystalline) wherein the number of series cells (N_s) for these modules were 54, 50 and 60, respectively. The experimental *I-V* data of the modules were retrieved from the previously reported parameters (Kler et al., 2017). The *I-V* characteristics at standard test condition (STC) together with the module parameters such as photocurrent (I_{phSTC}), open circuit voltage (V_{oc}), reverse saturation current (I_{oSTC}), series resistance (R_{sSTC}), shunt resistance (R_{shSTC}) and temperature coefficients for short circuit current (K_i) were utilized to produce the experimental *I-V* characteristics at different temperature and irradiation conditions following expressions:

$$I_\lambda = \frac{G}{G_{STC}}\left(I_{\lambda_{STC}} + K_i\Delta T\right) \qquad (20)$$

$$I_o = I_{o_{STC}} \left(\frac{T}{T_{STC}}\right)^3 \exp\left(\frac{qE_g}{nk}\left(\frac{1}{T_{STC}} - \frac{1}{T}\right)\right) \qquad (21)$$

$$R_{sh} = \frac{G_{STC}}{G} R_{sh_{STC}} \qquad (22)$$

$$R_s = R_{s_{STC}} \qquad (23)$$

$$V_{oc} = nV_t ln\frac{I_\lambda}{I_o} \qquad (24)$$

$$E_g = E_{g_{STC}}(1 - 0.0002677\Delta T) \qquad (25)$$

where G and T are the irradiance and temperature values at which the module need to be modelled. E_{gSTC} is the material bandgap at STC and is considered to be E_{gSTC} = 1.12 *eV* for silicon cells and E_{gSTC} = 1.6 *eV* for triple junction amorphous cells.

3.3.1 Temperature Analysis

In the first assessment, the modules with various cell temperatures of 25 °C, 50 °C and 75 °C at the fixed irradiance of 1000 W/m^2 were considered. The parameters extracted by BA with RMSE values for different module temperatures are summarized in Table 6. Results revealed that BA model could extract well the devices parameters at different temperatures with competitive accuracy. The proposed model outperformed the Hybrid Firefly and Pattern Search Algorithms (Beigi and Maroosi, 2018).

Table 6: Extracted parameters by BA for various solar modules operated at irradiance 1000 W/m^2 and different module temperatures.

Parameter	KC200GT	SX3200N	1STH-235-WH
***T* = 25 ºC**			
n (Ns×n)	1.1787(63.65)	1.0968(54.84)	1.0900(65.40)
R_s (Ω)	0.2699	0.2818	0.3648
R_{sh} (Ω)	177.506	724.340	1777.600
I_λ (A)	8.2213	8.9262	8.5394
I_o (A)	6.8857×10^{-9}	7.3834×10^{-8}	2.3535×10^{-9}
RMSE	47.6092×10^{-3}	13.1039×10^{-3}	12.9375×10^{-3}

***T* = 50 ºC**			
n ($N_s \times n$)	1.1080(59.83)	1.0775(53.87)	1.0982(65.89)
R_s (Ω)	0.3072	0.2902	0.3617
R_{sh} (Ω)	174.963	734.592	1679.890
I_λ (A)	8.3489	9.1513	8.7153
I_o (A)	4.5846×10^{-8}	1.4697×10^{-6}	7.2932×10^{-8}
RMSE	24.4609×10^{-3}	8.7261×10^{-3}	14.4952×10^{-3}
***T* = 75 ºC**			
n ($N_s \times n$)	1.0949(59.13)	1.0768(53.84)	1.0675(64.05)
R_s (Ω)	0.3114	0.2896	0.3768
R_{sh} (Ω)	175.016	1201.450	1253.930
I_λ (A)	8.4741	9.3724	8.8926
I_o (A)	6.0031×10^{-7}	2.5100×10^{-5}	7.3819×10^{-7}
RMSE	12.4216×10^{-3}	6.0655×10^{-3}	3.9505×10^{-3}

The experimental values and simulated/fitted curves of *I-V* characteristics for the modules at different cell temperatures are displayed in Figs. 9-11. The fitted *I-V* curves are shown to be in good agreement with the experimental ones over the entire range of the voltage records. Hence, BA model can be a competitive method to accurately extract the solar cells and modules parameters operating at various environmental conditions. Furthermore, an increase in the solar module's temperature led to an increase in the value of I_{sc} and reduced V_{oc}. The observed increase in I_{sc} with temperature was ascribed to the enhanced charge transport and increased generation current (I_o). Conversely, the reverse trend of V_{oc} change was attributed to the reduced p–n junction ability to separate electrons from holes in the photogenerated pairs. The ideality factor was dropped and approached unity with the rise of temperature, suggesting an improvement in the quality of charge transport within the semiconductor active layer of the devices. Furthermore, the parameters of the monocrystalline based solar module (1STH-235WH) were more sensitive to the temperature change compared to those of the multicrystalline ones (KC200GT and SX3200N). These findings were seen to be in good agreement with theoretical results and experimental observations (Chander et al., 2015; Cuce et al., 2013; Muhammad, Fahmi F. et al., 2017; Radziemska, 2003).

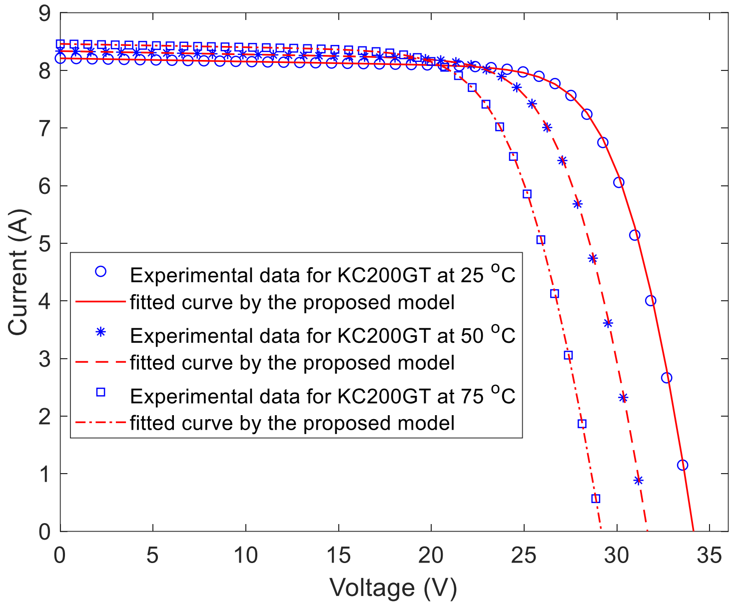

Fig. 9. Experimental and simulated *I-V* characteristics of KC200GT PV module worked at different temperatures

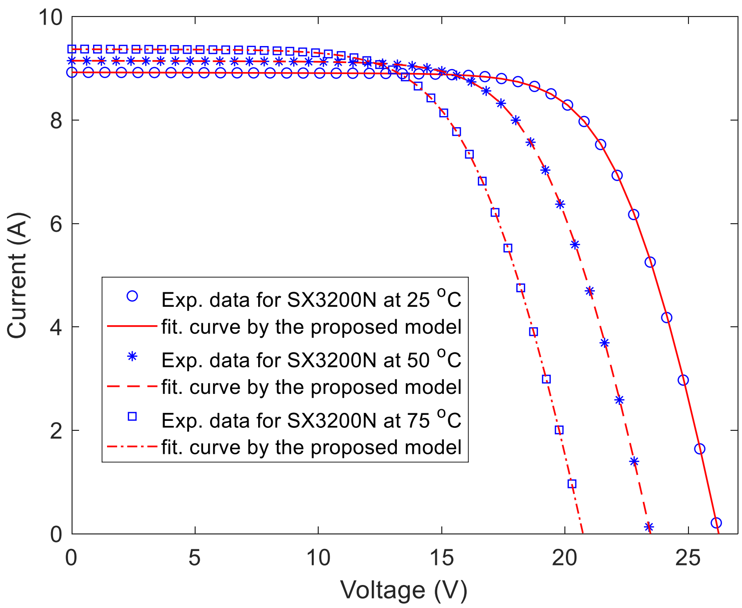

Fig. 10. Experimental and simulated *I-V* characteristics of SX3200N PV module operated at different temperatures

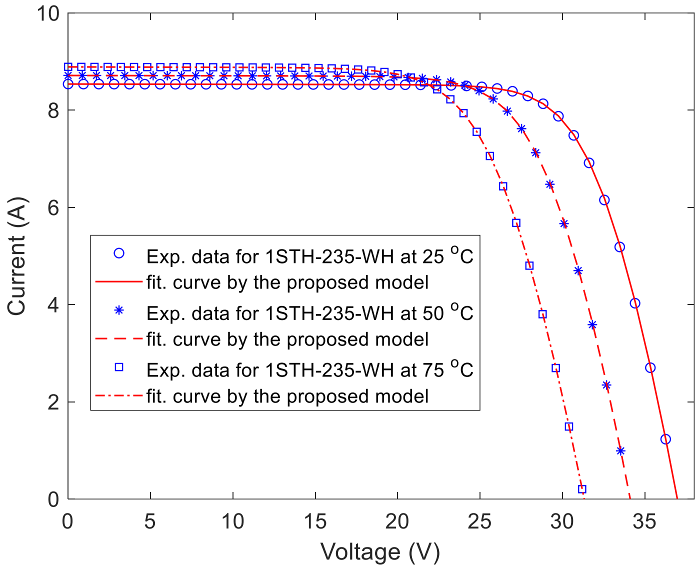

Fig. 11. Experimental and simulated *I-V* characteristics of 1STH-235-WH PV module operated at different temperatures

3.3.2 Irradiation Analysis

For the assessment of BA model under various irradiances, the experimental results of the three modules operated at constant temperature of 25 °C and changing irradiances such as 200 W/m^2, 600 W/m^2 and 1000 W/m^2 were considered. Table 7 summarizes the extracted parameters at different irradiances. Results showed that BA could achieve low RMSE when utilized to simulate the *I-V* characteristics of solar modules at varied irradiances. The comparison between experimental and model results for KC200GT, SX3200N and 1STH-235WH modules is illustrated in Figs. 12, 13, and 14, respectively. It is concluded that the proposed method can be relied on as a competitive model to simulate the *I-V* characteristics of solar cells and solar modules under different thermal and solar irradiation conditions, thereby extracting the five important parameters of single-diode model. The impact of increased illumination intensity on the PV parameters can be clearly seen, where V_{oc}, I_{sc} and P_m are simultaneously increased with the rise of solar irradiance. The overall trend was the improvement of the solar module's performance upon the rise of irradiation, thereby increasing the photogenerated current. Generally, the values of I_λ and I_o were found to enhance and R_s was reduced with the increase of illumination. However, there may be some deviations from these generalizations based on whether the modules are made from monocrystalline or multicrystalline semiconductor. In addition, the existence of some errors that may arise during experimental measurements and accuracy limitations of the proposed models used to import the modules parameters can lead to presence some discrepancies. For instance, experimental findings of Cuce et al. acknowledged that the ideality factor could decrease with the rise of illumination (Cuce et al., 2013). However, the model results displayed a reverse trend for the monocrystalline module (1STH-235WH), where the value of n was observed to increase with the increase of irradiance from 200 to 1000 W/m^2.

Table 7: Extracted parameters from BA for various solar modules operated at 25 ^{o}C and different solar irradiances.

Parameter	KC200GT	SX3200N	1STH-235-WH
G = 1000 W/m^2			
n ($Ns\times n$)	1.1787(63.65)	1.0968(54.84)	1.0900(65.40)
R_s (Ω)	0.2699	0.2818	0.3648
R_{sh} (Ω)	177.506	724.340	1777.600
I_λ (A)	8.2213	8.9262	8.5394
I_o (A)	6.8857×10^{-9}	7.3834×10^{-8}	2.3535×10^{-9}
RMSE	47.6092×10^{-3}	13.1039×10^{-3}	12.9375
G = 600 W/m^2			
n ($Ns\times n$)	1.0215(55.16)	1.1077(55.38)	0.9935(59.61)
R_s (Ω)	0.3285	0.2648	0.3911
R_{sh} (Ω)	225.533	1159.660	461.124
I_λ (A)	4.9365	5.3563	5.1291
I_o (A)	2.8012×10^{-10}	8.5715×10^{-8}	2.7885×10^{-10}
RMSE	16.7598×10^{-3}	18.1553×10^{-3}	25.1033×10^{-3}
G = 200 W/m^2			
n ($Ns\times n$)	0.8851(47.79)	1.0047(50.24)	0.8473(50.84)
R_s (Ω)	0.4195	0.3264	0.5758
R_{sh} (Ω)	364.442	1094.700	690.779
I_λ (A)	1.6464	1.7861	1.7098
I_o (A)	9.0884×10^{-12}	1.4427×10^{-8}	6.4094×10^{-12}

RMSE	21.5324×10^{-3}	5.3443×10^{-3}	18.0056×10^{-3}

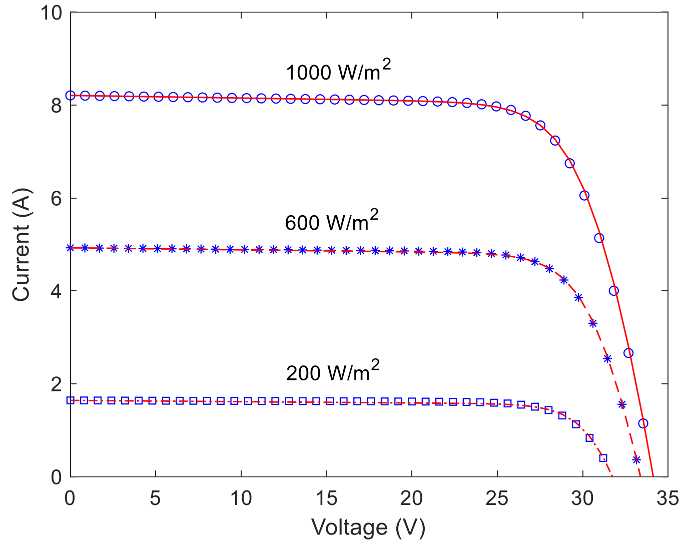

Fig. 12. Experimental (data points) and simulated (fitted curves) *I-V* characteristics of KC200GT PV module at different irradiances.

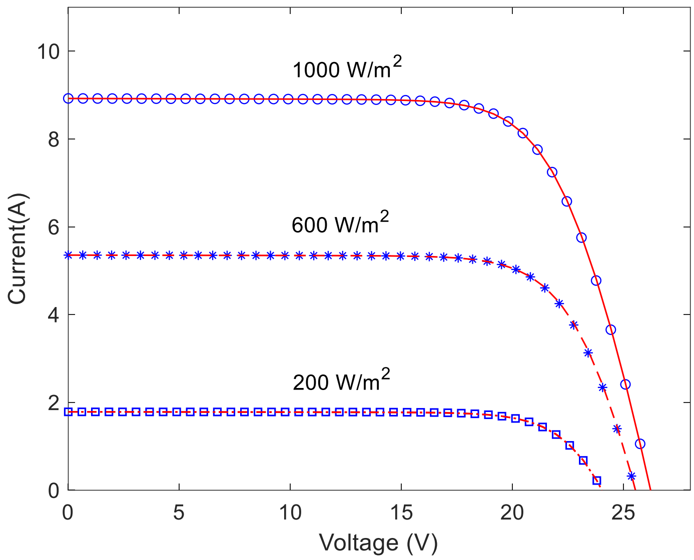

Fig. 13. Experimental (data points) and simulated (fitted curves) *I-V* characteristics of SX3200N PV module at different irradiances.

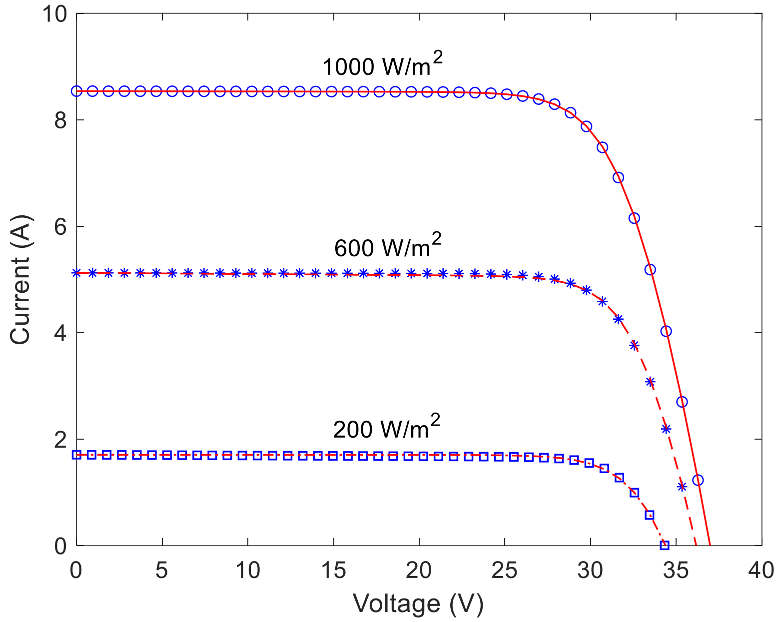

Fig. 14. Experimental (data points) and simulated (fitted curves) *I-V* characteristics of 1STH-235-WH PV module at different irradiances.

3.4 Sensitivity analysis and convergence speed

The algorithms used to extract solar cells and modules parameters are usually sensitive to some initializations and fitting parameters. Our proposed BA based algorithm utilizes a set of *I-V* data, in which the four PV parameters, V_{oc}, I_{sc}, V_m and I_m, are initially deduced by curve fitting, then they are used to extract the five PV cells/modules parameters. It was found that polynomial and Fourier curve fittings are well adopted to find each of V_{oc} and I_{sc}, respectively. However, we noticed that by changing the fitting type around P_m to extract V_m and I_m, it is possible to better compensate for efficient extraction of the cells/modules parameters. Table 8 presents the results of different fitting types that were used around P_m for the R.T.C. France solar cell and Photowatt-PWP-201 solar module. One can notice that the polynomial curve fitting has contributed to the lowest RMSE of parameters extraction for both of the PV devices. Consequently, the second-degree polynomial curve fitting was assigned to extract V_m and I_m for all the datasets investigated by the proposed algorithm.

Table 8. Utilization of different fitting types around P_m to show their effect on the efficiency of extracted PV cells and modules parameters.

	Fitting type	n	R_s (Ω)	R_{sh} (Ω)	I_λ (A)	I_o (μA)	RMSE
R.T.C. France solar cell	Gaussian	1.4630	0.0370	49.7426	0.7608	0.2690	8.2130×10^{-4}
	Polynomial	1.4732	0.0367	52.4722	0.7608	0.2983	$\mathbf{7.7897\times10^{-4}}$
	Spline	1.4690	0.0368	51.4048	0.7609	0.2866	8.7223×10^{-4}
	Fourier	1.4732	0.0367	52.4722	0.7608	0.2983	$\mathbf{7.7897\times10^{-4}}$
	Exponential	1.4853	0.0363	55.8511	0.7608	0.3348	1.4048×10^{-3}
	Power series	1.4853	0.0363	55.8511	0.7608	0.3348	1.4048×10^{-3}
	Sine	1.4146	0.0389	40.7110	0.7610	0.1658	5.1541×10^{-3}
Photowatt-PWP201 solar module	Gaussian	1.2905	1.2740	757.1040	1.0324	1.9242	2.2957×10^{-3}
	Polynomial	1.3357	1.2184	761.4900	1.0323	2.9984	$\mathbf{2.1256\times10^{-3}}$
	Spline	1.3811	1.2586	14866.10	1.0307	4.6453	6.1884×10^{-3}
	Fourier	1.3633	1.2240	1616.580	1.0314	3.9227	3.4522×10^{-3}
	Exponential	1.3924	1.1917	1791.930	1.0314	5.0988	3.5561×10^{-3}
	Power series	1.3311	1.3584	12254.20	1.0308	2.9250	8.1751×10^{-3}
	Sine	1.3554	1.2364	17.4322	1.0314	3.6504	3.7012×10^{-3}

Further investigation on the robustness of the proposed algorithm was carried out by changing the value of ideality factor while recording the values of other four parameters and RMSE simultaneously. That is because in our proposed approach, n is considered to be the only independent variable in Eq. (16), while the other four parameters are dependent on n. For instance, by giving a specific value to n, each of the R_s, R_{sh}, I_o and I_λ can be determined, respectively. Therefore, results of parameters extraction can be highly sensitive to the value of n. Consequently, it is imperative to initialize a range of n values with high decimals, by which the extraction of accurate parameters is guaranteed. It can be observed from Fig. 15 that there exists a unique minimum RMSE at which the parameters can be efficiently extracted. The intersection points of the curves with the vertical line passing through the lowest RMSE present the values of the parameters accordingly.

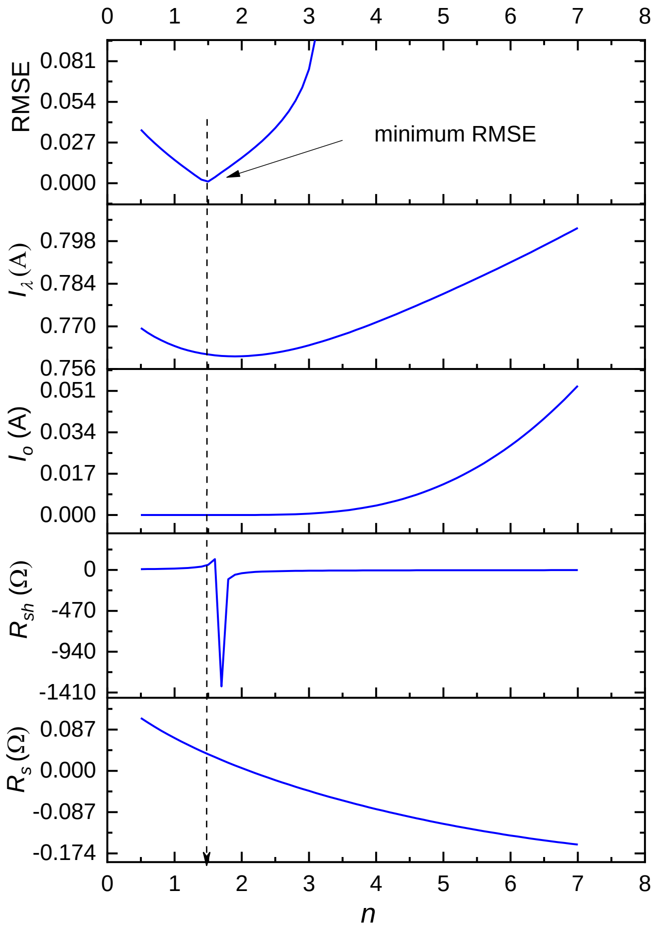

Fig. 15. Dependency of the parameters on *n* while extracting their values at lowest RMSE.

The sensitivity of the proposed algorithm to the percentage change in the PV cells/modules parameters was also analyzed by adding a relative error to each parameter from 10% to -10% in steps of 1% while keeping the other parameters constant. Table 9 shows the variation in RMSE between the measured and calculated currents for the R.T.C. France solar cell and Photowatt-PWP-201 solar module as a result of the error inclusion, while the number inside parenthesis presents the value of the corresponding parameter. Noticeably, the proposed method is more sensitive to the deviation in the values of n and R_s, with less sensitivity to each of I_λ, I_o and R_{sh}, respectively. It is worth to mention that by using the proposed technique, the values of n, R_s, I_λ and I_o are accurately extracted as the minimum RMSE was found to be located at 0% error of these parameters (Table 9). This extraction accuracy can be due to the consideration of n as the only independent variable in Eq. (16) to extract the rest of parameters, which is in agreement with the results presented in Fig. 15. Although the reduction in the value of R_{sh} has led to minimum RMSE at -2% and -5% of error for the solar cell and module, respectively, the presented errors are considered to be insignificant (≤0.05). As such, the proposed BA technique is capable of well extracting R_{sh} with trivially above the value at which RMSE is minimal. Consequently, a higher accurate value of R_{sh} can be deduced considering R_{sh}(1-0.02) and R_{sh}(1-0.05) for the solar cells and modules, respectively.

Table 9. Variation in RMSE when a systematic relative error of ±10% is presented to each of the extracted parameters individually.

Error (%)	**RMSE (Parameter value) for R.T.C. France solar cell**					**RMSE (Parameter value) for Photowatt-PWP201 solar module**				
	n	**R_s (Ω)**	**R_{sh} (Ω)**	**I_λ (A)**	**I_o (μA)**	***n***	**R_s (Ω)**	**R_{sh} (Ω)**	**I_λ (A)**	**I_o (μA)**
10	0.2205 (1.6205)	0.0048 (0.0404)	0.0011 (57.7194)	0.0678 (0.8369)	0.0207 (0.3281)	0.2910 (1.4693)	0.0090 (1.3402)	0.00288 (837.6390)	0.0859 (1.1355)	0.0275 (3.2982)
9	0.2059 (1.6058)	0.0043 (0.0400)	0.0011 (57.1947)	0.0610 (0.8293)	0.0187 (0.3251)	0.2691 (1.4559)	0.0081 (1.3281)	0.00282 (830.0241)	0.0774 (1.1252)	0.0248 (3.2683)
8	0.1898 (1.5911)	0.0038 (0.0396)	0.0010 (56.6700)	0.0543 (0.8217)	0.0166 (0.3223)	0.2457 (1.4426)	0.0073 (1.3159)	0.00275 (822.4092)	0.0689 (1.1149)	0.0221 (3.2383)
7	0.1723 (1.5763)	0.0034 (0.0393)	0.0009 (56.1453)	0.0475 (0.8141)	0.0146 (0.3192)	0.2208 (1.4292)	0.0064 (1.3037)	0.00268 (814.7943)	0.0604 (1.1046)	0.0194 (3.2083)
6	0.1531 (1.5616)	0.0029 (0.0389)	0.0009 (55.6205)	0.0407 (0.8064)	0.0125 (0.3162)	0.1943 (1.4158)	0.0056 (1.2915)	0.00262 (807.1794)	0.0519 (1.0942)	0.0167 (3.1783)
5	0.1323 (1.5469)	0.0024 (0.0385)	0.0009 (55.0958)	0.0340 (0.7988)	0.0105 (0.3132)	0.1662 (1.4025)	0.0048 (1.2793)	0.00260 (799.5645)	0.0434 (1.0839)	0.0139 (3.1483)
4	0.1097 (1.5321)	0.0020 (0.0382)	0.0008 (54.5711)	0.0272 (0.7912)	0.0084 (0.3102)	0.1365 (1.3891)	0.0040 (1.2671)	0.00253 (791.9496)	0.0349 (1.0736)	0.0112 (3.1183)
3	0.0852 (1.5174)	0.0016 (0.0378)	0.0008 (54.0464)	0.0204 (0.7836)	0.0063 (0.3072)	0.1051 (1.3758)	0.0033 (1.2550)	0.00246 (784.3347)	0.0264 (1.0633)	0.0084 (3.0884)
2	0.0589 (1.5027)	0.0012 (0.0374)	0.0008 (53.5216)	0.0137 (0.7760)	0.0042 (0.3043)	0.0719 (1.3624)	0.0027 (1.2428)	0.00244 (776.7198)	0.0179 (1.0529)	0.0058 (3.0584)
1	0.0305 (1.4879)	0.0009 (0.0371)	0.0008 (52.9969)	0.0069 (0.7684)	0.0022 (0.3013)	0.0371 (1.3491)	0.0024 (1.2306)	0.00233 (769.1049)	0.0094 (1.0426)	0.0033 (3.0284)
0	**0.0008** **(1.4732)**	**0.0008** **(0.0367)**	0.0008 (52.4722)	**0.0007** **(0.7608)**	**0.0007** **(0.2983)**	**0.0021** **(1.3357)**	**0.0021** **(1.2184)**	0.00229 (761.4900)	**0.0021** **(1.0323)**	**0.0021** **(2.9984)**
-1	0.0324 (1.4585)	0.0010 (0.0363)	0.0008 (51.9475)	0.0067 (0.7532)	0.0024 (0.2953)	0.0381 (1.3223)	0.0026 (1.2062)	0.00225 (753.8751)	0.0081 (1.0220)	0.0039 (2.9684)
-2	0.0671 (1.4437)	0.0014 (0.0360)	**0.0007** **(51.4228)**	0.0135 (0.7456)	0.0045 (0.2923)	0.0783 (1.3090)	0.0032 (1.1940)	0.00221 (746.2602)	0.0165 (1.0117)	0.0065 (2.9384)
-3	0.1039 (1.4290)	0.0018 (0.0356)	0.0008 (50.8980)	0.0203 (0.7380)	0.0066 (0.2894)	0.1203 (1.2956)	0.0039 (1.1818)	0.00217 (738.6453)	0.0250 (1.0013)	0.0093 (2.9084)

-4	0.1429	0.0023	0.0008	0.0271	0.0088	0.1641	0.0047	0.00215	0.0336	0.0122
	(1.4143)	(0.0352)	(50.3733)	(0.7304)	(0.2864)	(1.2823)	(1.1697)	(731.0304)	(0.9910)	(2.8785)
-5	0.1842	0.0027	0.0008	0.0338	0.0110	0.2098	0.0055	**0.00213**	0.0421	0.0152
	(1.3995)	(0.0349)	(49.8486)	(0.7228)	(0.2834)	(1.2689)	(1.1575)	**(723.4155)**	(0.9807)	(2.8485)
-6	0.2277	0.0032	0.0008	0.0406	0.0132	0.2572	0.0064	0.00214	0.0507	0.0181
	(1.3884)	(0.0345)	(49.3239)	(0.7152)	(0.2804)	(1.2556)	(1.1453)	(715.8006)	(0.9704)	(2.8185)
-7	0.2735	0.0037	0.0008	0.0474	0.0155	0.3064	0.0073	0.00215	0.0593	0.0211
	(1.3701)	(0.0341)	(48.7991)	(0.7075)	(0.2774)	(1.2422)	(1.1331)	(708.1857)	(0.9600)	(2.7885)
-8	0.3215	0.0042	0.0009	0.0542	0.0177	0.3574	0.0082	0.00216	0.0679	0.0242
	(1.3553)	(0.0338)	(48.2744)	(0.7000)	(0.2744)	(1.2288)	(1.1209)	(700.5708)	(0.9497)	(2.7585)
-9	0.3718	0.0047	0.0009	0.0610	0.0020	0.4102	0.0092	0.00218	0.0765	0.0272
	(1.3406)	(0.0334)	(47.7497)	(0.6923)	(0.2715)	(1.2155)	(1.1087)	(692.9559)	(0.9394)	(2.7585)
-10	0.4243	0.0052	0.0010	0.0678	0.0022	0.4648	0.0101	0.00221	0.0851	0.0303
	(1.3259)	(0.0330)	(47.2250)	(0.6847)	(0.2685)	(1.2021)	(1.0966)	(685.3410)	(0.9291)	(2.6986)

The presence of noise or error in the measured *I-V* data is another issue which acts upon reducing the sensitivity of the methods used to extract solar cells and modules parameters. In this context, a random noise with various relative errors was added to the experimental current data of R.T.C. France solar cell, as follows (Zhang et al., 2011):

$$I_{with\_noise} = I_{without\_noise}(1 + percent \times error) \qquad (26)$$

As such, the noisy data were used to extract device parameters with the proposed BA approach. Fig. 16 shows the percentage of relative error in the extracted parameters for different intensity of the typical random error. It was seen that when the noise relative intensity is 5%, the error for n is about 4%, while for R_s is about 4.6%, suggesting good stability of our proposed BA method under different experimental errors. It is known that calculated current is more sensitive to n, R_s and I_λ than R_{sh} and I_o (see Table 9). Therefore, the relatively high percentage error in the extracted I_0 and R_{sh} does not affect the validity of our proposed method.

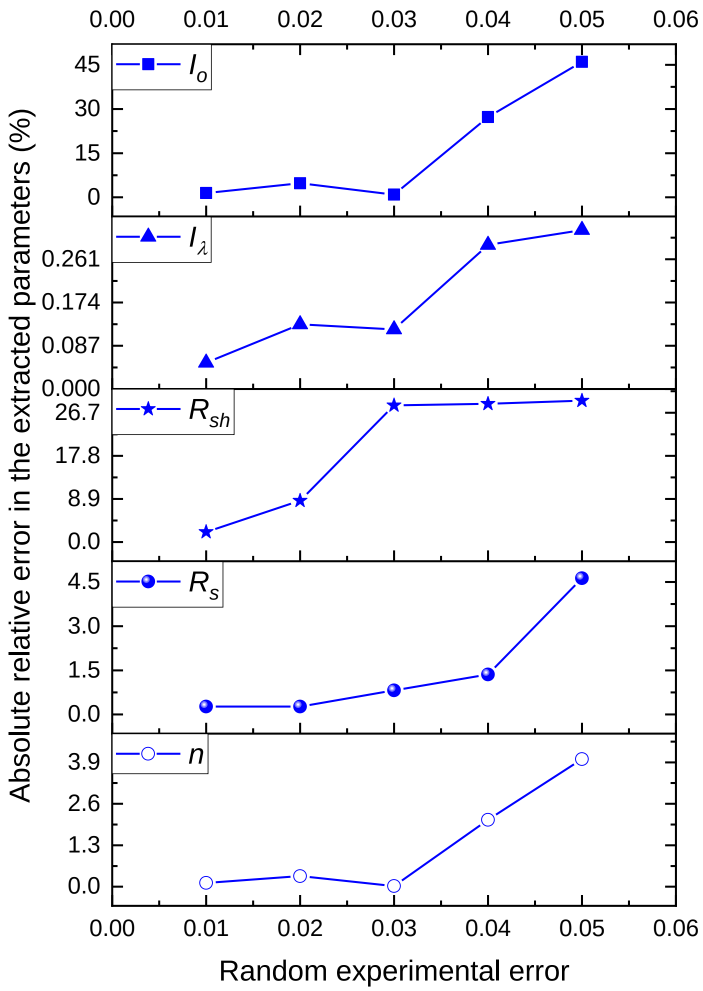

Fig. 16. The change in absolute relative error of the extracted parameters when a random error with different relative intensity is added to the experimental data.

In addition to the experimental errors arise in the measured *I-V*, there might be uncertainties in the measured irradiance and temperature of solar cells/modules. Hence, it is also interested to observe the impact of errors that are introduced by the outdoor conditions. Since PV cell temperature (T) is an inherent variable in the equation of single-diode modelling and presenting itself in almost all the equations, we made further investigations on the impact of error in the measured temperature on the extracted parameters. Nevertheless, a relatively linear effect of irradiance error on the deviation of PV cells/modules parameters can be noticed from Eq. (20) to Eq. (24). The change in relative error of the extracted parameters of R.T.C. France solar cell and Photowatt-PWP201 solar module with respect to the errors in measured temperature is shown in Fig. 17. One can notice that for the R.T.C. solar cell, over a broad range of temperature error from -5% to +5%, there exists a zero-relative error for all the extracted parameters except for the ideality factor, of which it is considered insignificant, since error < 5% (see Fig. 17(a)). However, this was seen to be different for the Photowatt-PWP201 solar module, where R_{sh} and I_o have been highly affected by the presence of error in measured T from 1% to 5%. This is where the introduction of a negative error, from -1% to -5%, has led to accurate extraction of R_{sh} and I_o with a zero-relative error. Therefore, it is concluded that the proposed BA method has a high tolerance to the error of measured temperature when it is applied to extract the solar cell parameters. It is worth to mention that PV cell's temperature need to be accurately measured in order to well extracting the device parameters, especially when PV modules are under investigation.

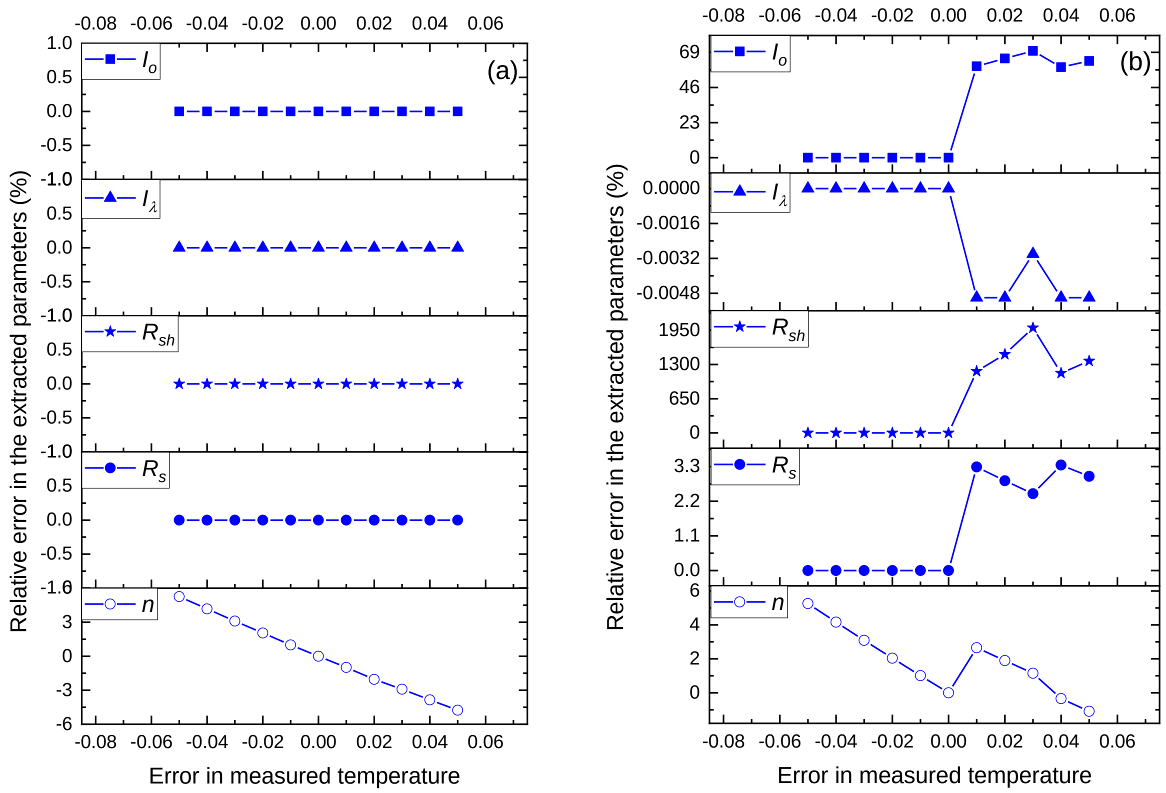

Fig. 17. The change in relative error of the extracted parameters of R.T.C. France solar cell (a) and Photowatt-PWP201 solar module (b) against error in the measured temperature.

Interestingly, by using the proposed BA approach, the whole process of parameters extraction takes few seconds. Fig. 18(a) shows that only seven iterations are sufficient to arrive at the best solution with a stable minimum RMSE between the experimental and calculated data. In each iteration, the tuning range of n is narrowed down towards the local minima while maintaining five decimal points for n in the final iteration. It is seen from Fig. 18(b) that less than one second is required to complete one iteration and hence the whole computation time is about 5 seconds. This indicates the fast convergence speed for the proposed BA based algorithm, thereby achieving low computational cost yet with high efficiency when it comes to extract the parameters of solar cells and modules parameters.

Achieving a right balance between the execution time and accuracy of parameters extraction are considered to be crucial for efficient modelling of solar cells and modules. Very recently, three-diode modelling was proposed as alternatives to the single-diode and double-diode modelling for industrial PV devices (Allam et al., 2016; Khanna et al., 2015). It was however claimed that three-diode model is capable of better interpreting the charge transport and recombination behaviours within the bulk active layer of these devices, the utilized algorithms used for the parameters extraction are time consuming and lose their ability to provide accurate solutions, especially with the increased number of the estimated parameters (Allam et al., 2016). Comparably, the single-diode model is well adopted to rapidly determine the conventional solar cell/module parameters without compromising on efficiency. However, it faces some limitations when it comes to extract the parameters of organic-based, Perovskite and dye-sensitized solar cells (Grätzel, 2003; Muhammad and Sulaiman, 2011; Snaith et al., 2014). This is because of the non-uniformly distributed series resistance in these types of PV devices, where interfacial behaviour and nano-phased donor-acceptor boundaries playing a major role in easily modifying the *I-V* shape compared to those of the inorganic solar cells.

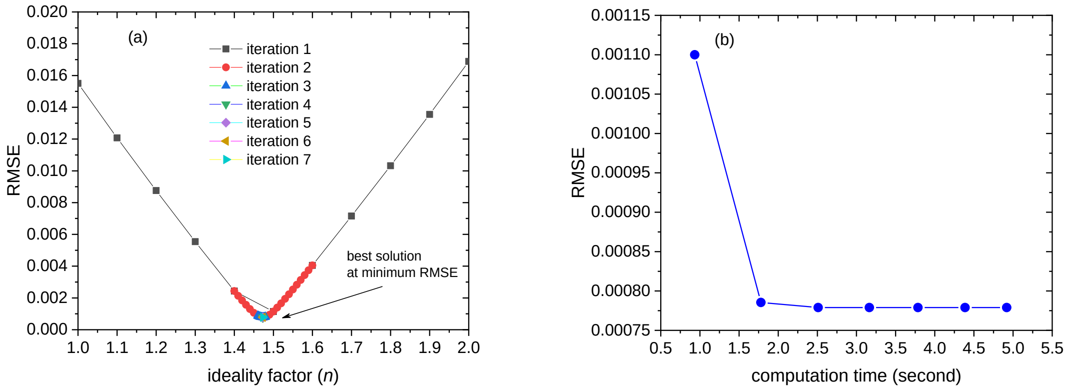

Fig. 18. Minimization of RMSE with the change of *n* per iteration (a) and computation time required for the whole process of parameters extraction within seven iterations (b).

3.5 Comparison with practically measured parameters

The proposed BA based method was also applied to extract parameters of blue and grey solar cells, thereby making a comparison with their practically measured parameters (Charles et al., 1981) and analytically extracted ones (Cubas et al., 2014b), as shown in Table 10. Noticeably, the extraction results showed great closeness of n, R_s, I_o and I_λ to the benchmark values. However, the extracted R_{sh} was seen to be trivially higher than that of the practically measured one. This can be due to the sensitivity characteristic of the proposed BA based approach which might be originated from the assumption of neglecting $\exp\left(\frac{R_s I_{sc}}{nV_t}\right)$ in the initially derived equations. Noteworthy, the higher error in the extracted R_{sh} compared to that of the other parameters does not affect the validity of our proposed method as it was previously demonstrated that calculated current is less sensitive to R_{sh} (see Table 9).

Table 10. Comparison of the extracted parameters for blue and grey solar cells

Device	Method	*n*	R_s (Ω)	R_{sh} (Ω)	I_λ (A)	I_o (A)
Blue SC	BA (proposed)	1.51±0.04	0.066±0.007	1104±15	0.1023±0.0001	$(110\pm10)\times10^{-9}$
	Practical/Benchmark (Charles et al., 1981)	1.51±0.07	0.07±0.009	1000±50	0.1023±0.0005	$(110\pm50)\times10^{-9}$
	Analytical (Cubas et al., 2014b)	1.51	0.0652	1093	0.1023	111×10^{-9}
Grey SC	BA (proposed)	1.72±0.06	0.08±0.01	26.5±0.3	0.5625±0.0002	$(5.41\pm1)\times10^{-6}$
	Practical/Benchmark (Charles et al., 1981)	1.72±0.08	0.08±0.01	26±1	0.5625±0.0005	$(6\pm3)\times10^{-6}$
	Analytical (Cubas et al., 2014b)	1.72	0.0781	26.25	0.5627	5.4×10^{-6}

4. Conclusions

A new approach was used on the single-diode equation for the simple and efficient extraction of the solar cells and modules parameters, thereby simulation of the *I-V* characteristics of these devices. This led to the derivation of a non-linear formula for R_s wherein BA was used to solve. The value of R_s was accurately estimated at every fine-tuned point of *n*, which was further used to determine all other devices parameters. The set of parameters having lowest RMSE value between the experimental and simulated *I-V* data were selected to be the best solution. The proposed BA based method was tested and validated on ten different solar cells and modules under diverse temperatures and irradiations. *I-V* simulation of R.T.C. France and PVM 752 GaAs solar cell revealed the lowest RMSE value of 7.79×10^{-4} and 2.11×10^{-4}, respectively. The Photowatt-PWP201, LEYBOLD 664 431 and STE 4/100 solar modules exhibited the respective RMSE value of 2.13×10^{-3}, 8.38×10^{-4} and 3.34×10^{-4}. The proposed BA model disclosed excellent performance when tested on various solar modules operated at different cell temperatures and under varied solar irradiations. In short, it outperformed several previously reported computational and heuristic algorithms used to extract the parameters of single-diode model for solar cells and solar modules under varying environmental conditions.

Acknowledgments

The authors sincerely thank the anonymous reviewers for their constructive comments which greatly improved the quality of this paper. The authors should also thank Universiti Teknologi Malaysia for the financial support under Vote No: Q.J090000.21A4.00D20 and Fahmi F. Muhammadsharif thanks Koya University for their administrative support during the implementation of this work.

Conflict of Interest

The authors declare that there is no conflict of interest regarding the publication of this work.

Appendices

Appendix A. Simulation results obtained using BA for single-diode model of R.T.C. France solar cell worked at 33 °C and irradiation of 1000 W/m^2.

Appendix B. Simulation results obtained via BA for single-diode model of PVM 752 GaAs thin film cell operated at 25 °C and irradiation of 1000 W/m^2.

Appendix C. Simulation results obtained using BA for single-diode model of Photowatt-PWP201 module comprised of 36 polycrystalline silicon cells in series operated at 45 °C and 1000 W/m^2.

References

Ahmad, Z., Touati, F., Muhammad, F.F., Najeeb, M.A., Shakoor, R., 2017. Effect of ambient temperature on the efficiency of the PCPDTBT: PC71BM BHJ solar cells. Applied Physics A 123(7), 486.

Allam, D., Yousri, D., Eteiba, M., 2016. Parameters extraction of the three diode model for the multi-crystalline solar cell/module using Moth-Flame Optimization Algorithm. Energy Conversion and Management 123, 535-548.

AlRashidi, M., AlHajri, M., El-Naggar, K., Al-Othman, A., 2011. A new estimation approach for determining the I–V characteristics of solar cells. Solar Energy 85(7), 1543-1550.

Askarzadeh, A., dos Santos Coelho, L., 2015. Determination of photovoltaic modules parameters at different operating conditions using a novel bird mating optimizer approach. Energy Conversion and Management 89, 608-614.

Askarzadeh, A., Rezazadeh, A., 2012. Parameter identification for solar cell models using harmony search-based algorithms. Solar Energy 86(11), 3241-3249.

Askarzadeh, A., Rezazadeh, A., 2013a. Artificial bee swarm optimization algorithm for parameters identification of solar cell models. Applied Energy 102, 943-949.

Askarzadeh, A., Rezazadeh, A., 2013b. Extraction of maximum power point in solar cells using bird mating optimizer-based parameters identification approach. Solar energy 90, 123-133.

Askarzadeh, A., Rezazadeh, A., 2013c. A new heuristic optimization algorithm for modeling of proton exchange membrane fuel cell: bird mating optimizer. International Journal of Energy Research 37(10), 1196-1204.

Bana, S ,.Saini, R., 2017. Identification of unknown parameters of a single diode photovoltaic model using particle swarm optimization with binary constraints. Renewable Energy 101, 1299-1310.

Beigi, A.M., Maroosi, A., 2018. Parameter identification for solar cells and module using a Hybrid Firefly and Pattern Search Algorithms. Solar Energy 171, 435-446.

Brent, R.P., 1971. An algorithm with guaranteed convergence for finding a zero of a function. The Computer Journal 14(4), 422-425.

Brent, R.P., 2013. Algorithms for minimization without derivatives. Courier Corporation.

Chaibi, Y., Salhi, M., El-jouni, A., Essadki, A., 2018. A new method to extract the equivalent circuit parameters of a photovoltaic panel. Solar Energy 163, 376-386.

Chander, S., Purohit, A., Sharma, A., Nehra, S., Dhaka, M., 2015. A study on photovoltaic parameters of mono-crystalline silicon solar cell with cell temperature. Energy Reports 1, 104-109.

Charles, J., Abdelkrim, M., Muoy, Y., Mialhe, P., 1981. A practical method of analysis of the current-voltage characteristics of solar cells. Solar cells 4(2), 169-178.

Chegaar, M., Ouennoughi, Z., Hoffmann, A., 2001. A new method for evaluating illuminated solar cell parameters. Solid-state electronics 45(2), 293-296.

Chellaswamy, C., Ramesh, R .2016 ,.Parameter extraction of solar cell models based on adaptive differential evolution algorithm. Renewable Energy 97, 823-837.

Chen, X., Yu, K., Du, W., Zhao, W., Liu, G., 2016. Parameters identification of solar cell models using generalized oppositional teaching learning based optimization. Energy 99, 170-180.

Chen, Y., Wang, X., Li, D., Hong, R., Shen, H., 2011. Parameters extraction from commercial solar cells I–V characteristics and shunt analysis. Applied Energy 88(6), 2239-2244.

Chen, Z., Wu, L ,.Lin, P., Wu, Y., Cheng, S., 2016. Parameters identification of photovoltaic models using hybrid adaptive Nelder-Mead simplex algorithm based on eagle strategy. Applied Energy 182, 47-57.

Chin, V.J., Salam, Z., Ishaque, K., 2015. An improved method to estimate the parameters of the single diode model of photovoltaic module using differential evolution, Electric Power and Energy Conversion Systems (EPECS), 2015 4th International Conference on. IEEE, pp. 1-6.

Cubas, J., Pindado, S., de Manuel, C., 2014a. Explicit expressions for solar panel equivalent circuit parameters based on analytical formulation and the Lambert W-function. Energies 7(7), 4098-4115.

Cubas, J., Pindado, S., Victoria, M., 2014b. On the analytical approach for modeling photovoltaic systems behavior. Journal of power sources 247, 467-474.

Cuce, E., Cuce, P.M., Bali, T., 2013. An experimental analysis of illumination intensity and temperature dependency of photovoltaic cell parameters. Applied Energy 111, 374-382.

Del Cueto, J., Rummel, S .2005 ,.Comparison of diode quality plus other factors in polycrystalline cells and modules from outdoor and indoor measurements, Conference Record of the Thirty-first IEEE Photovoltaic Specialists Conference, 2005. IEEE, pp. 511-514.

Domanski, K., Alharbi, E.A., Hagfeldt, A., Grätzel, M., Tress, W., 2018. Systematic investigation of the impact of operation conditions on the degradation behaviour of perovskite solar cells. Nature Energy 3(1), 61.

Easwarakhanthan, T., Bottin, J., Bouhouch, I., Boutrit, C .1986 ,.Nonlinear minimization algorithm for determining the solar cell parameters with microcomputers. International Journal of Solar Energy 4(1), 1-12.

Gaglia, A.G., Lykoudis, S., Argiriou, A.A., Balaras, C.A., Dialynas, E., 2017. Energy efficiency of PV panels under real outdoor conditions–An experimental assessment in Athens, Greece. Renewable energy 101, 236-243.

Gao, X., Cui, Y., Hu, J., Xu, G., Wang, Z., Qu, J., Wang, H., 2018. Parameter extraction of solar cell models using improved shuffled complex evolution algorithm. Energy Conversion and Management 157, 460-479.

Gong, W., Cai, Z., 2013. Parameter extraction of solar cell models using repaired adaptive differential evolution. Solar Energy 94, 209-220.

Grätzel, M., 2003. Dye-sensitized solar cells. Journal of photochemistry and photobiology C: Photochemistry Reviews 4(2), 145-153.

Guo, L., Meng, Z., Sun, Y., Wang, L., 2016. Parameter identification and sensitivity analysis of solar cell models with cat swarm optimization algorithm. Energy conversion and management 108, 520-528.

Hachana, O., Hemsas, K., Tina, G., Ventura, C., 2013. Comparison of different metaheuristic algorithms for parameter identification of photovoltaic cell/module. Journal of renewable and sustainable energy 5(5), 053122.

Hamid, N.F.A., Rahim, N.A., Selvaraj, J., 2016. Solar cell parameters identification using hybrid Nelder-Mead and modified particle swarm optimization. Journal of Renewable and Sustainable Energy 8(1), 015502.

Hu, X., Zou, Y., Yang, Y., 2016. Greener plug-in hybrid electric vehicles incorporating renewable energy and rapid system optimization. Energy 111, 971-980.

Humada, A.M., Hojabri, M., Mekhilef, S., Hamada, H.M., 2016. Solar cell parameters extraction based on single and double-diode models: A review. Renewable and Sustainable Energy Reviews 56, 494-509.

Ishaque, K., Salam, Z., 2011. An improved modeling method to determine the model parameters of photovoltaic (PV) modules using differential evolution (DE). Solar Energy 85(9), 2349-2359.

Jamadi, M., Merrikh-Bayat, F., Bigdeli, M., 2016. Very accurate parameter estimation of single-and double-diode solar cell models using a modified artificial bee colony algorithm. International Journal of Energy and Environmental Engineering 7(1), 13-25.

Jervase, J.A ,.Bourdoucen, H., Al-Lawati, A., 2001. Solar cell parameter extraction using genetic algorithms. Measurement Science and Technology 12(11), 1922.

Jordehi, A.R., 2018. Enhanced leader particle swarm optimisation (ELPSO): An efficient algorithm for parameter estimation of photovoltaic (PV) cells and modules. Solar Energy 159, 78-87.

Khanna, V., Das, B., Bisht, D., Singh, P., 2015. A three diode model for industrial solar cells and estimation of solar cell parameters using PSO algorithm. Renewable Energy 78, 1.113-05

Kler, D., Sharma, P., Banerjee, A., Rana, K., Kumar, V., 2017. PV cell and module efficient parameters estimation using Evaporation Rate based Water Cycle Algorithm. Swarm and Evolutionary Computation 35, 93-110.

Kumar, M., Kumar, A., 2017. An efficient parameters extraction technique of photovoltaic models for performance assessment. Solar Energy 158, 192-206.

Li, Z.-S., Zhang, G.-Q., Li, D.-M., Zhou, J., Li, L.-J., Li, L.-X., 2007. Application and development of solar energy in building industry and its prospects in China. Energy Policy 35(8), 4121-4127.

Louzazni, M., Aroudam, E.H., 2015. An analytical mathematical modeling to extract the parameters of solar cell from implicit equation to explicit form. Applied Solar Energy 51(3), 165-171.

Ma, T ,.Yang, H., Lu, L., 2014. Development of a model to simulate the performance characteristics of crystalline silicon photovoltaic modules/strings/arrays. Solar Energy 100, 31-41.

Magrab, E.B., Azarm, S., Balachandran, B., Duncan, J., Herold, K., Walsh, G .2007 ,. Engineers guide to MATLAB. Prentice Hall Press.

Maouhoub, N., 2018a. Photovoltaic module parameter estimation using an analytical approach and least squares method. Journal of Computational Electronics.

Maouhoub, N., 2018b. Photovoltaic module parameter estimation using an analytical approach and least squares method. Journal of Computational Electronics, 1-7.

McEvoy, A.J., Castaner, L., Markvart, T., 2012. Solar cells: materials, manufacture and operation. Academic Press.

Meneses-Rodríguez, D ,.Horley, P.P., Gonzalez-Hernandez, J., Vorobiev, Y.V., Gorley, P.N., 2005. Photovoltaic solar cells performance at elevated temperatures. Solar energy 78(2), 243-250.

Muhammad, F.F., Ketuly, K.A., Yahya, M.Y., 2018. Effect of Thermal Annealing on a Ternary Organic Solar Cell Incorporating Gaq3 Organometallic as a Boosting Acceptor. Journal of Inorganic and Organometallic Polymers and Materials 28(1), 102-109.

Muhammad, F.F., Sulaiman, K., 2011. Photovoltaic performance of organic solar cells based on DH6T/PCBM thin film active layers. Thin Solid Films 519(15), 5230-5233.

Muhammad, F.F., Sulaiman, K., 2018. Thermal Stability and Reproducibility Enhancement of Organic Solar Cells by Tris (hydroxyquinoline) gallium Dopant Forming a Dual Acceptor Active Layer .ARO-THE SCIENTIFIC JOURNAL OF KOYA UNIVERSITY 6(2), 69-78.

Muhammad, F.F., Yahya, M.Y., Hameed, S.S., Aziz, F., Sulaiman, K., Rasheed, M.A., Ahmad, Z., 2017. Employment of single-diode model to elucidate the variations in photovoltaic parameters under different electrical and thermal conditions. PLoS ONE 12(8), e0182925.

Muhammad, F.F., Yahya, M.Y., Sulaiman, K., 2017. Improving the performance of solution-processed organic solar cells by incorporating small molecule acceptors into a ternary bulk heterojunction based on DH6T: Mq3: PCBM (M= Ga, Al). Materials Chemistry and Physics 188, 86-94.

Müller, B., Hardt, L., Armbruster, A., Kiefer, K., Reise, C., 2016. Yield predictions for photovoltaic power plants: empirical validation, recent advances and remaining uncertainties. Progress in Photovoltaics: Research and Applications 24(4), 570-583.

Neubauer, C., Samieipour, A., Oueslati, S., Danilson, M., Meissner, D., 2019. Ageing of kesterite solar cells 1: Degradation processes and their influence on solar cell parameters. Thin Solid Films 669, 595-599.

Niu, Q., Zhang, H., Li, K., 2014. An improved TLBO with elite strategy for parameters identification of PEM fuel cell and solar cell models. International journal of hydrogen energy 39(8), 3837-3854.

Nunes, H ,.Pombo, J., Mariano, S., Calado, M., de Souza, J.F., 2018. A new high performance method for determining the parameters of PV cells and modules based on guaranteed convergence particle swarm optimization. Applied Energy 211, 774-791.

Oliva, D., Cuevas, E ,.Pajares, G., 2014. Parameter identification of solar cells using artificial bee colony optimization. Energy 72, 93-102.

Oliva, D., El Aziz, M.A., Hassanien, A.E., 2017. Parameter estimation of photovoltaic cells using an improved chaotic whale optimization algorithm. Applied Energy 200, 141-154.

Orioli, A., Di Gangi, A., 2016. A criterion for rating the usability and accuracy of the one-diode models for photovoltaic modules. Energies 9(6), 427.

Otte, K., Makhova, L., Braun, A., Konovalov, I., 2006. Flexible Cu (In, Ga) Se2 thin-film solar cells for space application. Thin Solid Films 511, 613-622.

Park, J.-Y., Choi, S.-J., 2015. A novel datasheet-based parameter extraction method for a single-diode photovoltaic array model. Solar Energy 122, 1235-1244.

Pindado, S., Cubas, J., 2017. Simple mathematical approach to solar cell/panel behavior based on datasheet information. Renewable energy 103, 729-738.

Pourmousa, N., Ebrahimi, S.M., Malekzadeh, M., Alizadeh, M., 2019. Parameter estimation of photovoltaic cells using improved Lozi map based chaotic optimization Algorithm. Solar Energy 180, 180-191.

Radziemska, E., 2003. The effect of temperature on the power drop in crystalline silicon solar cells. Renewable energy 28(1), 1-12.

Rasool, F., Drieberg, M., Badruddin, N., Singh, B.S.M., 2017. PV panel modeling with improved parameter extraction technique. Solar Energy 153, 519-530.

Senturk, A., Eke, R., 2017. A new method to simulate photovoltaic performance of crystalline silicon photovoltaic modules based on datasheet values. Renewable energy 103, 58-69.

Snaith, H.J., Abate, A., Ball, J.M., Eperon, G.E., Leijtens, T., Noel, N.K., Stranks, S.D., Wang, J.T.-W., Wojciechowski, K., Zhang, W., 2014. Anomalous hysteresis in perovskite solar cells. J. Phys. Chem. Lett 5(9), 1511-1515.

Tajuddin, M., Arif, M., Ayob, S., Salam, Z., 2015. Perturbative methods for maximum power point tracking (MPPT) of photovoltaic (PV) systems: a review. International Journal of Energy Research 39(9), 1153-1178.

Tong, N.T., Pora, W., 2 .016A parameter extraction technique exploiting intrinsic properties of solar cells. Applied energy 176, 104-115.

Verma, D., Nema, S., Shandilya, A., Dash, S.K., 2016. Maximum power point tracking (MPPT) techniques: Recapitulation in solar photovoltaic systems. Renewable and Sustainable Energy Reviews 54, 1018-1034.

Villalva, M.G., Gazoli, J.R., Filho, E.R., 2009. Comprehensive Approach to Modeling and Simulation of Photovoltaic Arrays. IEEE Transactions on Power Electronics 24(5), 1198-1208.

Villalva, M.G., Gazoli, J.R., Ruppert Filho, E., 2009. Comprehensive approach to modeling and simulation of photovoltaic arrays. IEEE Transactions on power electronics 24(5), 1198-1208.

Wei, H., Cong, J., Lingyun, X., Deyun, S., 2011. Extracting solar cell model parameters based on chaos particle swarm algorithm, Electric Information and Control Engineering (ICEICE), 2011 International Conference on. IEEE, pp. 398-402.

Xiao, W., Nazario, G., Wu, H., Zhang, H., Cheng, F., 2017. A neural network based computational model to predict the output power of different types of photovoltaic cells. PloS one 12(9), e0184561.

Yadir, S., Benhmida, M., Sidki, M., Assaid, E., Khaidar, M., 2009. New method for extracting the model physical parameters of solar cells using explicit analytic solutions of current-voltage equation, Microelectronics (ICM), 2009 international conference on. IEEE, pp. 390-393.

Ye, M., Wang, X., Xu, Y., 2009. Parameter extraction of solar cells using particle swarm optimization. Journal of Applied Physics 10.094502 ,(9)5

Yeh, W.-C., 2009. A two-stage discrete particle swarm optimization for the problem of multiple multi-level redundancy allocation in series systems. Expert Systems with Applications 36(5), 9192-9200.

Yıldıran, N., Tacer, E., 2016. Identification of photovoltaic cell single diode discrete model parameters based on datasheet values. Solar Energy 127, 175-183.

Yu, K., Liang, J.J., Qu, B.Y., Chen, X., Wang, H., 2017. Parameters identification of photovoltaic models using an improved JAYA optimization algorithm. Energy Conversion and Management 150, 742-753.

Yu, K., Qu, B., Yue, C., Ge, S., Chen, X., Liang, J., 2019. A performance-guided JAYA algorithm for parameters identification of photovoltaic cell and module. Applied Energy 237, 241-257.

Yuan ,X., Xiang, Y., He, Y., 2014. Parameter extraction of solar cell models using mutative-scale parallel chaos optimization algorithm. Solar Energy 108, 238-251.

Zagrouba, M., Sellami, A., Bouaïcha, M., Ksouri, M., 2010. Identification of PV solar cells and modules parameters using the genetic algorithms: Application to maximum power extraction. Solar energy 84(5), 860-866.

Zhang, C., Zhang, J., Hao, Y., Lin, Z., Zhu, C., 2011. A simple and efficient solar cell parameter extraction method from a single current-voltage curve. Journal of applied physics 110(6), 064504.

Zhang, Y., Lin, P., Chen, Z., Cheng, S., 2016. A population classification evolution algorithm for the parameter extraction of solar cell models. International Journal of Photoenergy 2016.